AN ABSTRACT OF THE THESIS OF

Joseph W. Coleman for the degree of Master of Science in Radiation Health Physics presented on June 10, 2003. Title: Determining Cross Sections for Potential Medical Radioisotopes.

Redacted for privacy

Abstract approved: _____

Stephen E. Binney

Cost effective medical isotope production is key to the success of many forms of radiation therapy. A lymphoma clinical trial for copper-67 was canceled in 1997 due to insufficient production quantities of the isotope (Fast Flux Test Facility, 2001). To date high flux thermal reactors and particle accelerator facilities have received the bulk of the production load; however, low flux thermal reactors can and should carry some of this load, perhaps even more economically in some cases. It is the primary goal of this research to demonstrate the viability of low flux thermal reactor medical isotope production.

A secondary premise of this research is to suggest that isotopes with the same desirable nuclear properties as those in widespread use have not been fully considered due to a lack of information. Simply put, medically important cross sections are either not known or are not known with a reasonable degree of certainty. Four potential medical radionuclides were identified as lacking sufficient cross section data. These

cross sections were measured to confirm or update older data and remove some of the "uncertainty."

The four isotopes identified as having desirable nuclear and chemical characteristics to serve as medical isotopes are: scandium-47 ($^{47}$Sc), copper-67 ($^{67}$Cu), yttrium-91 ($^{91}$Y), and the metastable state of tin-117 ($^{117m}$Sn). Irradiation methods were designed to isolate both epithermal and thermal reaction cross section data, as well as unfold the fast flux (fission spectrum) since three of the reactions are neutron-proton threshold reactions. Samples were irradiated and counted, and the reaction cross section values were calculated from the measured activity. Values were then compared to accepted values to determine if further study is warranted.

Production of medical isotopes in a thermal reactor can be a viable alternative and merits further comparative study. Three of the four reactions studied produced appreciable amounts of potential medical isotopes over a short irradiation period of three megawatt-hours, the exception being $^{91}$Y.

With little knowledge of the actual OSTR flux profile, a methodology was proven to "pin" the profile and accurately measure cross sections. The fission average cross section for the $^{67}$Zn(n,p) reaction of 1.07 ± 0.113 mb (one sigma) was found to be exactly the same as the widely adopted value. $^{47}$Ti(n,p) yielded a 15.5 ± 1.6 mb (one sigma) fission average cross section, which is slightly less than the ENDF/B-VI value of 22.4 mb. These results support the conclusion that medical isotope production in thermal reactors is feasible and continued research is warranted.

# Determining Cross Sections for Potential Medical Radioisotopes

by
Joseph W. Coleman

A THESIS

submitted to

Oregon State University

in partial fulfillment of
the requirements for the
degree of

Master of Science

Presented June 10, 2003
Commencement June 2004

Master of Science thesis of Joseph W. Coleman presented on June 10, 2003.

APPROVED:

Redacted for privacy

Major Professor, representing Radiation Health Physics

Redacted for privacy

Head of the Department of Nuclear Engineering and Radiation Health Physics

Redacted for privacy

Dean of the Graduate School

I understand that my thesis will become part of the permanent collection of Oregon State University libraries. My signature below authorizes release of my thesis to any reader upon request.

Redacted for privacy

Joseph W. Coleman, Author

# ACKNOWLEDGEMENTS

Dr. Stephen Binney for his continued support of me and my education. As my undergraduate advisor and now my Master Professor, I have always appreciated the opportunity to work with and learn from him.

To Dr. Kenneth Krane and doctoral candidate Christopher Staples from the Department of Physics for their collaboration on portions of this research and willingness to provide much needed "sanity checks" for my results.

To the faculty, staff and students of the Department of Nuclear Engineering and Radiation Health Physics at Oregon State University for providing a wealth of knowledge, guidance and assistance. Particularly, Dr. Steve Reese and Dr. Todd Palmer for taking time to share their insights in their areas of expertise applicable to my research.

To the United States Navy for their support of my graduate education.

Finally and most importantly, to my wife Evalyn and daughters Elinor, Isabel, and Margaret for their patience, support, and – most of all – their love.

TABLE OF CONTENTS

TABLE OF CONTENTS (continued)

Page

TABLE OF CONTENTS (continued)

LIST OF FIGURES

LIST OF TABLES

LIST OF TABLES (continued)

**Determining Cross Sections**
**for Potential Medical Radioisotopes**

## ABSTRACT

Cost effective medical isotope production is key to the success of many forms of radiation therapy. A lymphoma clinical trial for copper-67 was canceled in 1997 due to insufficient production quantities of the isotope (Fast Flux Test Facility, 2001). To date high flux thermal reactors and particle accelerator facilities have received the bulk of the production load; however, low flux thermal reactors can and should carry some of this load, perhaps even more economically in some cases. It is the primary goal of this research to demonstrate the viability of low flux thermal reactor medical isotope production.

A secondary premise of this research is to suggest that isotopes with the same desirable nuclear properties as those in widespread use have not been fully considered due to a lack of information. Simply put, medically important cross sections are either not known or are not known with a reasonable degree of certainty. Four potential medical radionuclides were identified as lacking sufficient cross section data. These cross sections were measured to confirm or update older data and remove some of the "uncertainty."

The four isotopes identified as having desirable nuclear and chemical characteristics to serve as medical isotopes are: scandium-47 ($^{47}$Sc), copper-67 ($^{67}$Cu), yttrium-91 ($^{91}$Y), and the metastable state of tin-117 ($^{117m}$Sn). Irradiation methods were designed to isolate both epithermal and thermal reaction cross section data, as

well as unfold the fast flux (fission spectrum) since three of the reactions are neutron-proton threshold reactions. Samples were irradiated and counted, and the reaction cross section values were calculated from the measured activity. Values were then compared to accepted values to determine if further study is warranted.

Production of medical isotopes in a thermal reactor can be a viable alternative and merits further comparative study. Three of the four reactions studied produced appreciable amounts of potential medical isotopes over a short irradiation period of three megawatt-hours, the exception being $^{91}Y$.

With little knowledge of the actual OSTR flux profile, a methodology was proven to "pin" the profile and accurately measure cross sections. The fission average cross section for the $^{67}Zn(n,p)$ reaction of $1.07 \pm 0.113$ mb (one sigma) was found to be exactly the same as the widely adopted value. $^{47}Ti(n,p)$ yielded a $15.5 \pm 1.6$ mb (one sigma) fission average cross section, which is slightly less than the ENDF/B-VI value of 22.4 mb. These results support the conclusion that medical isotope production in thermal reactors is feasible and continued research is warranted.

# INTRODUCTION

## 1.1 BACKGROUND

> "Each year, U.S. physicians employ radioisotopes in an estimated 13 million nuclear-medicine procedures and another 100 million laboratory tests. Most of these activities rely on only a few nuclides, principally iodine-131 and technetium-99m.
>
> During the past 5 years, the goals of nuclear medicine have been expanding. Instead of just diagnosing diseases, the field has begun to target the treatment of disorders. This shift has spurred exploration of dozens of uncommon isotopes.
>
> Last year, DOE convened an expert panel to forecast what future U.S. demand for unconventional medical isotopes might be if research were to proceed unimpeded. It found that use of these, including unconventional therapeutic isotopes, could grow 7 to 14 percent per year. In 20 years, the fledgling therapeutic nuclear-medicine industry could be valued at as much as $1.1 billion annually, it found." (Raloff, 1999)

Janet Raloff eloquently puts into perspective the urgency of this type of research. A promising clinical trial for $^{67}Cu$ cancer treatment was terminated because of a lack of accelerator time for production (Fast Flux Test Facility, 2001). Using national lab accelerator facilities for production of research medical isotopes is central to the problem. Securing the necessary "accelerator time" gets bogged down in the quagmire of budget constraints and competing experiments – all the more reason to research the possibility of low flux thermal reactor production of medical isotopes.

For the most part, cross section data have been derived from studies designed to benefit reactor design and nuclear weapons programs. Many of the available cross section data were measured in the infancy of nuclear power and some measurements are over fifty years old (McLane, 1988). Since that time nuclear medicine and

diagnostic imaging have made great strides by putting the available information to good use. However, it is important to realize that by comparison only a relatively few studies have focused on medical isotopic production. Much of the isotopic cross section data listed in many of the "current" libraries was derived with antiquated equipment and, more importantly, with another end in mind.

Shifting the focus to the efficient and cost effective production of useful medical isotopes causes a necessary shift in methodology and exactitude of information. Designing irradiation experiments that target a particular reaction for a specific isotope leads to less ambiguous results. Using germanium detectors has also improved the accuracy and precision of cross section results. The coupled effects of the germanium detectors and more precise methods will result in a more certain cross section value. More accurate information will permit a more informed decision regarding the feasibility of an isotope for a particular medical application and may lead to further investigation.

Medical isotope production is becoming increasingly important from both a financial and medical benefits perspective. As previously noted by Raloff (1999), this is big business, yet the corresponding research funding is not necessarily well targeted. Most of the monies are targeted at the pharmaceutical end, or the delivery system, with a comparatively small amount directed toward finding new and better production methods for radioisotopes. There seems to be a large degree of what may prove to be misplaced trust in the data that provides a basis for these types of decisions. At this point it will be useful to review some key points in selecting a medical isotope.

## 1.2 CRITERIA FOR MEDICAL ISOTOPE SELECTION

Four basic criteria are considered in selecting the best radioisotopes for medical applications. These are half-life, decay mode and energy, production reaction cross section, and the availability of a pharmaceutical delivery label. *Half-li*fe is the time it takes for 1/2 of the activity to decay away. *Decay mode and energy* refer to the mechanism of decay; that is, to say the type of particle emitted and the energy released in that decay. Measurement of the production reaction *cross section*, or the probability of production under a neutron flux, is the focus of this research. Attachment of the radioisotope to *pharmaceutical delivery label*, called radiolabeling, to facilitate in-vivo transport to the region of interest is the last criterion to be satisfied.

### 1.2.1 HALF-LIFE

First and foremost, medical isotopes must have a half-life that is not too short and not too long. A half-life on the order of a few hours is optimal for most imaging applications. This allows adequate time to produce an image while minimizing the dose from post-imaging in-vivo decay. From a manufacturing standpoint, a shorter half-life reduces the amount of time from the point of production to the point of application, which can lead to delivery issues. After five half-lives the radiopharmaceutical has decayed away to approximately 3% of its initial activity.

Assuming the case of a radioisotope with a half-life of one hour, there is a window of less than five hours during which time a useful amount of radioactivity for

imaging or therapy exists. In about a two to four hour period, the radioisotope must be delivered from the isotope production facility to the pharmaceutical lab where it is labeled with the delivery pharmaceutical before it is delivered to the medical facility for use on patients. Sometimes the radiolabels are "attached" at the patient care facility, which saves some time; however, this practice is less common as the radiopharmaceutical manufacturers become more efficient in all facets of production.

Obviously a longer half-life would eliminate the "rush" of production and delivery, but then once administered to a patient it would result in a larger dose. Normal biological removal methods are slow when compared to the radioactive decay removal factor for shorter-lived radionuclides. An isotope with a two hour half-life would deliver the major portion of the dose to the body for a period of over ten hours, when only a few hours are needed to get the desired image.

The balance between minimizing patient dose and maximizing production and delivery time requires the use of an isotope with a moderate half-life relative to the desired irradiation period. Since half-lives are generally well known, this serves as a good initial argument for selection of suitable radionuclides.

### 1.2.2 DECAY MODE AND ENERGY

Another important factor is the decay mode and energy of the radionuclide. This selection criterion is entirely dependent on the imaging technique or type of therapy regimen. For example, if it is desired to uptake a beta emitter for dose

delivery to a tumor, then it would make sense to only consider radionuclides that primarily beta ($\beta^-$) decay. The energy of the emitted $\beta^-$ is important in determining the dose depth. The more energetic the $\beta^-$ particles, the deeper they will penetrate into tissue as the $\beta^-$ energy is dissipated and dose is delivered. Similarly, most imaging techniques are most effective using low energy photons (x-rays or gamma rays) emitted from a specific organ, or tumor, to paint a three dimensional picture of the region of interest. Photon energies of $\sim 150$ keV are ideal for managing

### 1.2.3 REACTION CROSS SECTION

The criteria of half-life and decay mode and energy can be readily employed to develop a comprehensive list of potential medical isotopes. However, these are not the only criteria used; otherwise, the perfect choice may be a radioisotope that is nearly impossible to produce. It must be cost effective in terms of the amount of activity produced for a given irradiation time and flux. Cost analysis will not be directly performed here, but can be inferred by the magnitude of the fission average cross section. A larger cross section yields a greater production rate for a given flux.

Whether or not it is "cost effective" will depend on how well the demand for the medical isotope compares to the production rate. If the demand far exceeds the rate of production then another means of production must be sought or another isotope used that can be more easily produced. Since the cross section is a physical property and cannot be changed, the flux is the variable tweaked to increase production rates.

The choice between an accelerator, a high-energy reactor, high-flux thermal reactor, or low-flux thermal reactor is directly linked to the production demand and the size of the cross section. Another way of putting it is to say that reaction rates drive production rates.

Reaction rates for a given neutron flux and sample mass are determined by the reaction probability, or cross section. Unfortunately, most of the available cross section data was derived many years ago with antiquated techniques, counting, and computing systems. Moreover, the cross sections were not determined with a focus on medical applications; rather, they were a byproduct of early reactor analysis and nuclear weapons programs. If discovery of new medical isotopes is important to the continued progress in patient care, then it is imperative that these cross section values are more precisely determined. This will ensure that all of the best possible radionuclides are considered using the most accurate information available.

It may be that the best isotopes for a wide range of medical applications have yet to be discovered simply because a fifty year old cross section value has erroneously led to their elimination from further consideration. It is a goal of this research to demonstrate through use of modern counting systems and techniques that poorly known cross sections can be more precisely calculated. Several isotopes with poorly known cross sections have been selected based on otherwise desirable properties. It is the hope, although not the immediate goal, that this research will lead to the discovery of more medical isotopes that were previously discounted due to poorly known cross sections or the inability to produce them in sufficient quantities.

### 1.2.4 PHARMACEUTICAL RADIOLABELING

Once the choice is made of isotopes with acceptable half-lives, desired modes of decay and energies, and a cross section that enhances production capabilities, the ubiquitous question of finding an appropriate carrier pharmaceutical becomes central to the problem. This is not a question that is considered by this research. If all of the above criteria are met, then the research to discover the pharmaceutical that will one day be attached to deliver new radioisotopes to regions of interest in the body will naturally follow. Without meeting the preceding criteria, however, there is no need for this research. Therefore, so as to not put the cart before the horse, more precise knowledge of the fission average cross section is necessarily the primary concern in the discovery of the next generation of medical isotopes.

# LITERATURE REVIEW

## 2.1 GENERAL REVIEW OF CROSS SECTION MEASUREMENTS

In literature there exists a wealth of information regarding nuclear reaction cross section measurements, and not every researcher conducts these types of experiments in the same way or in the same facility. A brief review of some of the preeminent sources in the field of neutronics and nuclear data measurements is in order to ensure that this work is fully understood and ambiguity is put aside.

Several resources, while not contributing directly to the results, have provided necessary background for the comparisons and evaluations made by this report.

- Duderstadt et al. (1976) provides a simplified, but comprehensive, review of cross section derivation and calculation tailored for the Nuclear Engineer.
- Mughabghab et al. (1981) gives a much more detailed description tailored to the Nuclear Physicist, as well as a wealth of cross section data used in various forms in this research.

There are several ways to report cross section measurements, which, if compared to one another without an understanding of how each value is calculated, could lead to meaningless conclusions.

### 2.1.1 MICROSCOPIC CROSS SECTION DEFINED

Microscopic cross section is simply the probability a neutron-nuclear interaction will occur. The units of $cm^2$ imply that a cross section is an area measurement – this is only partially true. While the physical cross sectional area a nucleus presents to an incident neutron is part of the probability of an interaction, it does not distinguish the probability of a particular reaction nor does it represent the ability of the nucleus to absorb, even for a short time, another neutron. The cross section represents a probability that is analogous to a pseudo-target-area presented to an incident neutron. It depicts the likelihood that a particular reaction (e.g., neutron-proton or neutron-gamma) will occur, which may in fact be much larger or smaller than the physical cross sectional area ($\pi r^2$) of the nucleus.

### 2.1.2 INTEGRAL AND DIFFERENTIAL CROSS SECTION MEASUREMENT

Many cross section experiments have measured cross section values at specific energies using charged particle accelerators; this is termed the differential method. An integral method would be an experiment conducted in a reactor over a continuum of energies. The integral method is the more circuitous experimental procedure, as it requires unfolding the reactor flux to measure the cross sections. Given that most (n,p) reactions occur well above thermal and epithermal neutron energies, proper flux unfolding is the key to achieving accurate results.

Fewer neutrons compounded by smaller cross sections deter most researchers from using the integral method for threshold reaction experiments, but both the integral and differential methods are important and agreement between the two is essential to data validation. Either method, when correctly employed, should result in the same average cross section. An average cross section is calculated using a function that describes the neutron distribution as a function of energy in a reactor. This function tends to weight the true cross section more at energies with more neutrons, and less at energies with fewer neutrons.

### 2.1.3 CROSS SECTION DATABASE LIBRARIES

Having a basic understanding of the numerous cross section database libraries and the experimental procedures used to measure such data will prove helpful in assessing the validity of the results of this research. All libraries are a variation of the Evaluated Nuclear Data File (ENDF) maintained by the National Nuclear Data Center (NNDC) at the Brookhaven National Laboratory (BNL). Only the ENDF will be discussed, but its general description holds true for most of the others as well.

It is important distinguish the word "evaluated" in this title to mean that a standard was employed when accepting new data – the data were *evaluated.* If specified methodologies and sound experimental practices, including error analysis, are adhered to, then the data will be included in the ENDF.

The current version, ENDF/B-VI (Release 8), includes the most recent scientific *evaluations* of the base library of "raw data" maintained by the NNDC. Several national groups use computer codes to input this raw data and generate an energetic continuum of reaction cross section values, including the NNDC. In the case of NNDC, the data are then referred to as "Evaluated ENDF Data". The purpose of this evaluation is quite different from the initial evaluation.

Initial data evaluation ensures it meets pre-established accuracy and precision standards and only qualifies it as acceptable raw data, while subsequent evaluations fit curves to the data filling in the gaps between measured data points. This greatly enhances the utility of the data to users, who are typically engineers and physicists. Most of the evaluated ENDF libraries are readily accessible through the Internet (see Appendix for a listing and description of those used in this research).

A cursory review of the evaluated ENDF tables will show that there are several forms in which a measured cross section can be reported. The convention is to select a known standard flux profile that closely approximates the thermal, epithermal, or fission energy spectrum. Regardless of the actual flux distribution in a reactor, one of these archetypal functions will be used to average, or weight, the cross section and will be reported as such in the tables (i.e., Maxwellian cross section, 1/E cross section, or fission average cross section). The NNDC has an evaluated Watt fission spectrum used to weight fission average cross sections. These flux profiles will be discussed in detail in the next section.

### 2.1.4 ARCHETYPAL FLUX PROFILES

The neutron energy spectrum in a reactor can be simplified by breaking it up into three distinct energy bands. The behavior of neutrons interacting with core materials (fuel, moderator, and control rods) is described using these energy bands. The first energy band is often referred to as a thermal neutron energy spectrum and is well modeled by the Maxwell-Boltzmann distribution for ideal gases (commonly referred to as the "Maxwellian distribution"). The lower bound of the thermal neutron energy range theoretically tends to zero, although neutrons of zero energy do not exist. It can be shown that neutrons in thermal equilibrium with their surroundings have a most probable energy of 1/2kT (typically ~0.0084 eV), where k is the Boltzmann constant and is equal to $8.6 \times 10^{-11}$ MeV/K, and T is the absolute temperature of the medium in Kelvin. 3/2kT (~0.0253 eV) is the average thermal neutron energy at room temperature with a corresponding velocity of 2,200 m/s (Binney, 1987).

The upper bound of the thermal energy band, 0.5 eV, is the lower bound of the epithermal energy band and is somewhat arbitrarily chosen based on the cadmium neutron absorption cross section "cutoff" energy. The epithermal neutron energy region is generally modeled using a 1/E fit. The epithermal, or resonance region as it is sometimes called, is bounded at 100 keV at which point the fast neutron band begins. The fast neutron spectrum continues to approximately 15 MeV. Although neutrons of higher energy can be born from fission, they rarely exceed 10 MeV (Duderstadt, 1976). The Watt equation predicts that less than 0.1% exceed 11 MeV

(Bresesti, 1970). 14.918 MeV, or 0.4 lethargy units above 10 MeV (ASTM, 1998), is often used as the upper limit for reactor neutronic calculations and will be used in the present research.

The fast neutron fission spectrum for uranium-235 is closely approximated by the Watt equation and is referred to as the Watt Fission Spectrum (WFS). The WFS is most accurate above energies of 1 MeV and has a most probable energy of ~ 0.72 MeV and an average energy of 2 MeV (Binney, 1987). Given that three of the reactions studied in this research are threshold reactions occurring near 2 MeV and above, the WFS was used extensively to profile the fission energy spectrum in the OSTR.

It should be noted that the energy bounds of 0.5 eV and 100 keV are arbitrarily chosen and do not strictly define the region for resonance behavior. In other words, every resonance for every material does not occur between 0.5 eV and 100 keV, yet this band is generally accepted as the limits of integration for evaluating resonance integrals (RI). The significance of standardizing the bounds of the epithermal band becomes apparent when considering the use of a flux monitor of moderate Z material, such as $^{54}Fe$, to calculate the cross section for a higher Z material, such as $^{91}Zr$. As material Z, increases the resonance region shifts to lower energies; conversely, as Z decreases, the resonance region shifts to higher energies.

Caution must be exercised when selecting a cross section for a flux monitor to ensure that its RI was calculated over the 0.5 eV to 100 keV range in accordance with the ASTM standard (1998). Some published RI values were derived by integration

over the entire observed resonance region and may not clearly annotate this subtle, but important, distinction. Obviously, using the proper RI is critical to the accuracy of the experimental results. More to the point, there were three different values for the $^{58}Fe(n,\gamma)^{59}Fe$ flux monitor reaction and *all* were correct. General Electric's Chart of the Nuclides list 1.2 b (1996); Mughabghab et al. list 1.7 b (1981); and the ASTM standard lists 1.479 b (1998). Only the ASTM standard clearly states: "Resonance integral uses a 1/E function for the source term and uses the integration limits of 0.5eV to 100 keV."

Standard neutron energy bands are important to prevent a "moving target" when attempting to fix a RI to an energy band. Furthermore, it is imperative that any deviations from the standard are explicitly annotated in sufficient detail to permit the data is used within the correct parameters.

### 2.1.5 AVERAGE CROSS SECTION MEASUREMENT

As in doubles tennis, when two players who individually are not "ranked" come together to produce marvelous results, the product of an energy integrated neutron fluence and cross section are similarly better together than they are apart. When the values are separated, that is, when a known average cross section is used to derive an unknown average flux or vice versa, the "known" value's actual energy dependence may not be known exactly. Moreover, even if it is known to a fair degree of precision, it is probably not the same as that of the measured product, since it was

most likely measured in a different neutron field. It is, however, assumed to adhere to one of the widely accepted neutron energy distributions, such as the Maxwell-Boltzmann Distribution (MBD) or the Watt Fission Spectrum (WFS) as previously discussed. It must always be remembered that these distributions are approximations to model reactor neutronics, and if a more detailed knowledge of the flux profile is required, then neutron transport computer codes should be used to mitigate the effects of any in-core perturbations.

Radioactivation techniques in a reactor force one to deal with a spectrum of neutron energies, as opposed to a monoenergetic beam from an accelerator. Real constraints, such as detector location, the presence of scattering and absorbing materials, and other similar effects result in perturbations in the otherwise pure fission energy distribution of neutrons. It is this difference in the flux between reactors that makes cross section analysis difficult. Researchers take comfort in knowing that the cross section does not change, only the flux.

The product of the energy integrated spectrum flux and cross section can be accurately measured without precisely knowing the flux. This "product" is essentially the reaction rate per target atom and can be directly calculated from the measured activity. It also brings solace to the researcher that most of the other parameters involved in the activity calculation have little or no energy dependence. Cross section data are generally derived empirically based on the relationship between the reaction rate, cross section, and flux (Equation 2.1).

$$\dot{R} = N \frac{\int \sigma(E)\varphi_w(E)dE}{\int \varphi_w(E)dE} \int \varphi_a(E)dE \qquad (2.1)$$

$\dot{R}$ ≡ reaction rate
$\sigma(E)$ ≡ energy dependent cross section
$\varphi_w(E)$ ≡ weighting function of energy dependent fluence
$\varphi_a(E)$ ≡ actual function of energy dependent fluence

As can be seen in the second factor of Equation 2.1, when calculating an average cross section, the integration over the energy spectrum for the flux is in both the numerator and denominator. This has the effect of averaging the cross section such that the flux shape is preserved but the magnitude is essentially normalized. Typically, a Maxwellian (thermal neutrons), 1/E (epithermal neutrons), or Watt (fission neutrons) distribution is used for $\varphi_w(E)$ in this integration. This helps to standardize the factor with the greatest variance between experiments – the flux.

While this goes a long way to standardizing tabulated values, the third factor in Equation 2.1 is also very important. This is the actual flux, $\varphi_a(E)$, incident upon the sample and is typically not known exactly. Transport computer codes can approximate this profile and other weighting techniques can be used to mitigate the variations from one spectrum to another. Simply put, the exact solution to this integral is difficult to know for a given reactor and can only be closely approximated.

Without the use of a conventionally known flux profile, $\varphi_w(E)$, to average the cross section, the resultant measurement would be unique to the flux profile in which it was measured and offer little utility to facilities without the same flux profile. This

research will follow convention and formulate results comparable to tabulated values, such that an "apples to apples" comparison is possible.

## 2.2 SPECIFIC REVIEWS

Each reaction considered in this work will be reviewed from two perspectives. First, the nuclear characteristics of the reaction and the emitted radiation will be detailed, including available cross section information. Secondly, the medical significance of the product radioisotope will be explained.

### 2.2.1 $^{117}Sn(n,\gamma)^{117m}Sn$

As is typically the case for neutron-gamma reactions, this reaction is an exothermic reaction (Q-value = 7.743 MeV). Of the reactions studied, this is the only reaction that occurs at thermal and epithermal neutron energies to any appreciable degree. Production of $^{117m}Sn$ from both the thermal and epithermal neutron capture reactions was studied.

#### 2.2.1.1 $^{117}Sn(n,\gamma)$ CROSS SECTION

Mausner et al. (1992) concluded that using a low flux thermal fission reactor to prepare $^{117m}Sn$ is only practical if enriched $^{116}Sn$ is used due to its low thermal cross

section. The same research also found that the 6 mb thermal cross section only produced a saturation specific activity of 74 MBq/mg (2 mCi/mg) in the Oak Ridge National Laboratory High Flux Isotope Reactor ($\varphi_{th} = 2.5 \times 10^{15}$ n/cm$^2$s). When dealing with very small cross sections, the optimal answer is to "turn up" the fluence. The book Neutron Cross Sections (Mughabghab, 1981) also lists a thermal cross section of 6 mb, as well as a resonance integral of 490 mb.

### 2.2.1.2 $^{117m}$Sn NUCLEAR PROPERTIES OF MEDICAL SIGNIFICANCE

$^{117m}$Sn ($t_{1/2}$ = 13.6 d) decays via internal conversion. Two conversion electrons of 126.8 keV (64.8%) and 151.6 keV (26.1%) comprise the major particles emitted (Kocher, 1981). Mausner et al. (1992) adds that an imagable photon of 158.6 keV (86.4 %) is also present.

The intended medical application is "relieving bone pain in breast and prostate cancer patients" (Mausner, 1992). The reduced range, ~ 0.2 mm in water, of the 126.8 keV electron leads to a more localized dose, which is vital in bone palliation applications. The majority of the dose deposition will be in the bone mineral where it is taken up, and to a lesser extent in the more radiosensitive bone marrow. Radiolabels already exist that can deliver the $^{117m}$Sn isotope to the bone mineral, and studies of the radiopharmaceutical being administered to patients have been conducted (Mausner, 1992).

### 2.2.2 $^{47}Ti(n,p)^{47}Sc$

This reaction, too, is an exothermic reaction (Q-value = 0.1823 MeV). Neutron-proton reactions occur primarily in the fast flux region of the neutron energy spectrum. Production of $^{47}Sc$ requires neutron energies above the thermal and epithermal energy ranges; hence, although the Q-value is positive, it is termed a *threshold reaction*, because it only occurs significantly for incident neutron energies above a certain threshold.

#### 2.2.2.1 $^{47}Ti(n,p)$ CROSS SECTION

A method was convolved to take tabulated data and average it over a Watt fission spectrum to obtain a rough fission spectrum average cross section for comparison to calculated values averaged in a similar manner. Essentially, the cross section for each tabulated energy was multiplied by a normalized WFS fraction evaluated at the same energy. These weighted cross sections were summed to provide a rough estimate of the average fission cross section. This is rough because it is a summation of finite points with varying energy widths ($\Delta E$), as opposed to a summation of points with a constant energy mesh. Using this method and the raw data provided in the Smith and Meadows (1975) report, a fission spectrum average cross section of ~ 21 mb was calculated using the Watt equation as the averaging function.

Smith and Meadows (1975) plotted results indicate an observed reaction threshold of just under 2 MeV, as this is where the cross section drops to a near zero value. An incident neutron of 1.9 MeV energy also corresponds to a quantum mechanical coulomb barrier transmission probability of one-percent. Coulomb barriers and quantum mechanical thresholds will be discussed in detail in Chapter 3.

Philis et al. (1977) use much of Smith and Meadows' data to construct the cross section plot below 10 MeV and extrapolate it to zero. Numerical methods were used to extrapolate the existing data to higher energies as well. A fission average cross section of 21.38 mb was reported with an estimated uncertainty of "5 to 10 percent below 10 MeV and somewhat larger at higher energies (Philis, 1977)."

Mannhart (1989) joined with Smith and Meadows to publish a report that was used to correct some deficiencies in the then "soon to be released" ENDF/B-VI data relating to this particular reaction. Specifically, their purpose was to resolve disagreement between cross section measurements evolved from using the differential versus the integral method. One significant provision taken by Mannhart et al. (1989) was to calibrate the Ge(Li) detector to within one percent of the low 159 keV photon energy. Another similar stipulation was that all, both the integral and differential, samples were counted on the same detector. That study determined the fission average cross section to be 18.2 b, which was 18% lower than the 22.45 mb value tabulated in the upcoming ENDF/B-VI release. Both cross section values were averaged using the ENDF Watt spectrum (Mannhart, 1989).

### 2.2.2.2 $^{47}$Sc NUCLEAR PROPERTIES OF MEDICAL SIGNIFICANCE

$^{47}$Sc decays 100% of the time via β- emission to either a first excited state or the ground state with a 3.35 day half life (Baard, 1989). The $\beta^-$ particles have maximum energies of 439 keV (68.4 %) and 600 keV (31.6%), and the 159.38 keV γ-ray emitted in immediate transition from the first excited state to the ground state is ideal for imaging applications. It is high enough energy to exit the body, low enough to interact with a detector crystal, and can easily be collimated or shielded (Binney, 2002). Having both an imagable γ-ray and tumor killing $\beta^-$-particles make this an excellent isotope for radioimmunotherapy (RIT) where a patient is injected with the $^{47}$Sc isotope, which is attached to a monoclonal antibody that preferentially seeks out tumors to deliver a deadly dose of radiation.

### 2.2.3 $^{67}$Zn(n,p)$^{67}$Cu

This is also an exothermic threshold reaction (Q-value = 0.2058 MeV) occurring in the fast flux region of the neutron energy spectrum. Production of $^{67}$Zn in a thermal reactor is expectedly difficult due to its very low (~1 mb) cross section coupled with it essentially being a threshold reaction. O'Brien (1969) reported an "effective threshold" of 4.7 MeV. The vernacular of "threshold" would suggest the point at which the reaction is energetically possible; however, an "effective threshold" has a decidedly different meaning. It is used to mean the energy at which the cross

section has risen to an appreciable level and the reaction is now "more likely" rather than only "energetically possible". More to the point, it has little to do with whether or not the reaction is energetically possible. This point is significant because in a thermal reactor small cross sections at lower energies are more heavily weighted in importance since that is where the bulk of the neutrons are available to drive the reaction. Threshold energy determination will be discussed further in Chapter 3.

### 2.2.3.1 $^{67}$Zn(n,p) CROSS SECTION

Previous research for this reaction was difficult to find. O'Brien (1969) is somewhat dated and there exists no *evaluated* ENDF file for this reaction. The raw ENDF data that have been submitted to the NNDC are available and were used to calculate a rough fission spectrum average cross section of ~ 2 mb as previously described.

Mirzadeh et al. (1986) is more current research, but is heavily slanted towards production in a high flux reactor or with an accelerator due to the small cross section at low neutron energies. Mirzadeh et al. (1986) measured the fission average cross section to be 1.23 mb, and noted that this was in "fair agreement with the adopted value of 1.07 mb." O'Brien (1969) experimentally determined the $^{67}$Zn(n,p) fission average cross section to be 0.82 ± 0.04 mb. His report also listed several other fission average cross sections from research conducted earlier than his own, which are listed

in Table 2.1. This was useful since there is a lack of available information on this reaction and evaluated data in standard cross section libraries are non-existent.

Table 2.1. Fission average cross section values listed in O'Brien's report (1969).

| Researcher Name(s) | $^{67}Zn(n,p)^{67}Cu$ Fission Average Cross Section | Flux Monitor (Basis for Measurement) |
|---|---|---|
| Passell and Health | 57 mb | 60 mb for $^{27}Al(n,\alpha)^{24}Na$ |
| Mellish et al. | 54 mb | 60 mb for $^{32}S(n,p)^{32}P$ |
| Shikata | 1.2 mb | 90 mb for $^{58}Ni(n,p)^{58}Co$ |

### 2.2.3.2 $^{67}$Cu NUCLEAR PROPERTIES OF MEDICAL SIGNIFICANCE

Like $^{47}$Sc, $^{67}$Cu is a $\beta^-$ emitter with a 62 hr half-life. The maximum $\beta^-$ energies are 577 keV (20%) to the ground state, 484 keV (23%) to the first excited state, and 395 keV (56%) to the second excited state (Lederer, 1978). The primary $\gamma$-ray emissions are 91.3 keV (7.3%), 93.3 keV (16.6%), and 184.6 keV (46.7%); these are suitable energies for imaging purposes. Similar to $^{47}$Sc, $^{67}$Cu has both an imagable $\gamma$-ray and tumor killing $\beta^-$-particles that make it an excellent isotope for RIT as well. Mirzadeh et al. (1986) describes the medical benefit as follows:

> "Copper-67 is an attractive nuclide radionuclide for therapy with radiolabeled tumor associated monoclonal antibodies. Typically such antibodies require 1-2 days to attain maximum concentration in the tumors. It is advantageous to use a nuclide with a half-life comparable to the uptake and residence time on the tumor. This also minimizes the non-target dose during the clearance phase of the antibody. The 62.01 hr half-life of $^{67}$Cu is sufficient for optimal tumor uptake."

### 2.2.4 $^{91}Zr(n,p)^{91}Y$

This is an endothermic threshold reaction (Q-value = -0.7625 MeV) occurring in the fast flux region of the neutron energy spectrum. Production of $^{91}Zr$ in a thermal reactor is expectedly difficult for the same reasons $^{67}Cu$ was difficult, but even more so. It, like $^{67}Cu$, has a very low (< 1 mb) cross section; however, the fact that it is an endothermic reaction with a kinematic threshold of ~770 keV leads to a higher quantum threshold. Also, zirconium has more protons than the other isotopes studied and, consequently, a larger Coulomb barrier, which pushes the threshold for this reaction even higher. As a point of clarification, the threshold discussed here is the energy at which the reaction becomes energetically possible. As previously discussed, *effective* thresholds tend to be higher. Again, in thermal reactors small cross sections at lower energies (where more neutrons exist) cannot be ignored. Based on the plot, the observed (not *effective*) threshold for this reaction is approximately 4.5 MeV, which is in excellent agreement with the calculated one-percent quantum threshold of 4.6 MeV.

#### 2.2.4.1 $^{91}Zr(n,p)$ CROSS SECTION

Qaim (1989) conducted a cross section measurement of all zirconium radioisotopes, including the $^{91}Zr(n,p)^{91}Y$ and the $^{91}Zr(n,p)^{91m}Y$ reactions. The present research did not measure the partial cross section to the metastable state since, $^{91m}Y$

has a 49.7 minute half-life and the sample was permitted to decay to ground state over a period of approximately 2 days prior to counting. The fission average cross section was not reported as part of Qaim's research, but was approximated from the plotted values using a normalized Watt fission spectrum as the averaging function. The approximate value is 2.4 mb over an energy range of 6.0 to 10.6 MeV (Qaim, 1989). This is a factor of ten greater than the evaluated ENDF/B-VI value of 0.26 mb due to the fact that all of the data points were above 6 MeV where only about 2.5% of thermal fission neutrons exist as predicted by the Watt equation (Bresesti, 1970).

### 2.2.4.2 $^{91}$Y NUCLEAR PROPERTIES OF MEDICAL SIGNIFICANCE

$^{91}$Y is another pure $\beta^-$ emitter with a 58.5 hr half-life (Lederer, 1978). It has a metastable state with a 49.7 minute half-life that decays to ground state via emission of a 555 keV $\gamma$-ray. $^{91}$Y $\beta^-$ decays (99.7%) to the ground state with a maximum $\beta^-$ energy of 1.54 MeV. This isotope has a very similar decay scheme and $\beta^-$ energy to $^{89}$Sr, a medical isotope currently used for cell-directed tumor therapy, a form of RIT. Compared to $^{47}$Sc and $^{67}$Cu, the slightly higher energy $\beta^-$ allows for a deeper dose deposition for larger tumors or use in less radiosensitive organs.

# MATERIALS AND METHODS

## 3.1 OVERVIEW

The main objective of this research is to assess the feasibility of medical isotope production in thermal reactors. To this end, the neutron cross sections of the greatest projected need to the future production of medical isotopes have been identified. Specifically, the cross sections leading to the production of $^{47}Sc$, $^{67}Cu$, $^{91}Y$, and $^{117m}Sn$ in a thermal fission reactor are to be measured. This effort involves calculation-based assessment and experimental verification of cross section data. Evaluations of existing integral data from previous investigators provided one basis for determining the accuracy of the cross sections derived from this research. The data will be processed and statistics developed to yield one-sigma errors on the values determined. Irradiation experiments will be performed at the Oregon State TRIGA Reactor (OSTR) to confirm the results of the integral data unfolding.

## 3.2 ISOTOPES IDENTIFIED

An evaluation of previous studies helped determine badly needed cross section measurements in support of the projected high production demand of medical radioisotopes. Final determination of isotopes from among all candidates was influenced by the availability of existing data, the cost of target materials, and the

likelihood of achieving adequate production levels of the isotopes. In this regard, medical isotopes that have not been generally available for research or application have been emphasized for study.

## 3.3 OSTR IRRADIATION FACILITY (ICIT AND CLICIT)

An OSTR irradiation facility (Figure 3.1) specifically designed for application of the cadmium difference method was used to calculate thermal and epithermal flux.

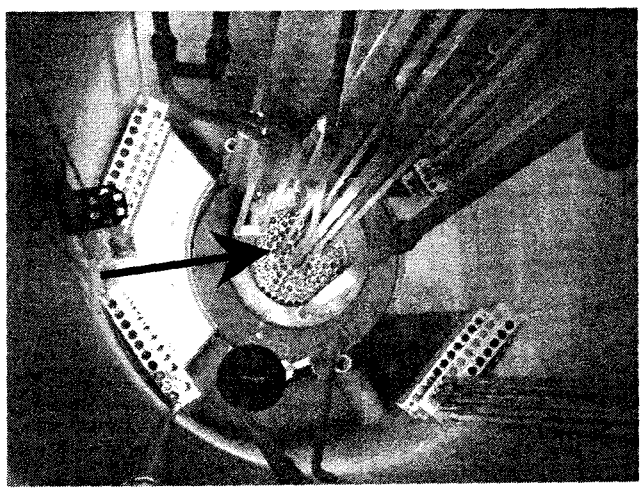

Figure 3.1. Photo of TRIGA reactor pool. Arrow is pointing to the Cadmium Lined and bare In Core Irradiation Tubes (CLICIT and ICIT). Photo courtesy of Oregon State Department of Nuclear Engineering and Radiation Health Physics.

The In-Core-Irradiation-Tube, called the "ICIT", is permeable to both the thermal and epithermal flux components. The Cadmium-Lined-In-Core-Irradiation-Tube, called the "CLICIT", is used to isolate the epithermal component by attenuating the low energy, or thermal, component of the neutron flux. According to the cadmium

difference method, the CLICIT flux is subtracted from the ICIT flux to find the thermal flux contribution. This method is well known and standardized by the American Society for Testing and Materials (ASTM) (1998).

ASTM (1998) and several other sources cite 1 mm as the standard thickness corresponding to sufficient removal of thermal neutrons or, more expressly, establishes a cadmium cutoff energy ($E_{Cd}$) of 0.5 eV. As the name "cutoff energy" implies, neutrons below 0.5 eV, the lower bound of the arbitrarily chosen epithermal range, are essentially removed from the flux profile as they are selectively absorbed by the cadmium shield. In fact, the removal fraction calculated (using Equation 3.1) for thermal neutrons passing through a 1.0 mm cadmium shield is about 99.999 %.

$$(1 - I/I_o) = 1\text{-}\exp(-N*\sigma*x), \text{ where } N = N_A*\rho /AW \qquad (3.1)$$

$(1\text{-}I/I_o) \equiv$ removal fraction
$\sigma \equiv$ microscopic cross section
$N \equiv$ number density
$N_A \equiv$ Avogadro's Number
$\rho =$ density
$x =$ thickness
$AW =$ atomic weight

The OSTR CLICIT facility deviates slightly from the ASTM standard with a 0.020 inch, or 0.508 mm, thick cadmium lining. Incidentally, the result of decreasing the thickness from 1.0 to 0.5 mm results in a removal fraction of 99.735%, or an increase of only 0.26% more thermal neutrons passing into the CLICIT – still a negligible number. The 0.5 mm cadmium thickness is supported by Knoll (1979) as

an appropriate thickness for the cadmium difference method where he states an $E_{Cd}$ of 0.4 eV.

It is important to realize that the energy value reported with each thickness is not related to the thickness inasmuch as it relates to the energy dependence of the cross section. Furthermore, a simple inspection of the cadmium absorption cross section versus energy plot shows a steep decline from ~ 7000 to ~ 7 b over the span from 0.1 to 5 eV (McLane, 1988); for that reason, an $E_{Cd}$ of either 0.4 or 0.5 eV is reasonable. Therefore, it is determined that the difference in the thickness of the cadmium lining will have negligible effect on the results and will be ignored.

## 3.4 SAMPLES WEIGHED, IRRADIATED, AND COUNTED

Elemental samples of each of the isotopes studied plus iron and nickel, which were used as a flux monitors, were irradiated. The samples were divided into two complete sets and each weighed prior to irradiation. The source of error in the weight and time measurements were considered negligible relative to the random errors associated with Neutron Activation Analysis (NAA).

One set was irradiated in the OSTR's ICIT and the other in the CLICIT. The TRIGA reactor was operated at full power (1 MW) for three hours to optimize the neutron field incident upon the samples without over-activating the samples, thereby maximizing the size of the resultant decay peaks observed.

Once irradiated the samples were given several days to "cool off" such that short-lived activity had decayed away and did not interfere with the gamma decay peaks of interest. Samples were then counted using germanium detectors. Spectral analysis was used to identify each peak associated with the isotopes of interest.

## 3.5 GAMMA SPECTROMETRY CROSS SECTION MEASUREMENTS

Count data from each peak were recorded. Reaction cross sections were calculated using a variation of the general Equation 3.2. Uncertainties in each term were recorded to provide for a rigorous error analysis of the resultant cross section.

$$\sigma_{rxn} \approx A_o/[N\,(1-\exp(-\lambda\, t_{irr}))\,\varphi_{rxn}], \tag{3.2}$$

where $N = [(m_{sample}/1000)/AW]\, f_{iso}\, N_a$

and $A_o = \lambda\, C/[\varepsilon\, I_\gamma \exp(-\lambda\ t_d)\,(1-\exp(-\lambda\ t_c))]$

$\sigma_{rxn} \equiv$ average reaction neutron cross section (b)
$\varphi_{rxn} \equiv$ average neutron flux over range of reaction ($cm^{-2}s^{-1}$)
$A_o \equiv$ initial activity at end of irradiation (dps)
$N \equiv$ total number of atoms of element
$\lambda \equiv$ decay constant ($s^{-1}$)
$m_{sample} \equiv$ mass of sample (mg)
$AW \equiv$ atomic weight (grams of element/mole)
$f_{iso} \equiv$ isotopic abundance fraction (atoms of isotope/atoms of element)
$N_a \equiv$ Avogadro's Number (atoms/mole)
$C \equiv$ net counts
$\varepsilon \equiv$ detector efficiency
$I_\gamma \equiv \gamma$-ray intensity fraction
$t_{irr} \equiv$ irradiation time (s)
$t_d \equiv$ decay time (s)
$t_c \equiv$ count time (s)

### 3.5.1 NEUTRON-GAMMA REACTIONS

The only neutron-gamma cross section value sought in this research involves the primary mode of production of $^{117m}Sn$: $^{116}Sn(n,\gamma)^{117m}Sn$. The small capture cross section of $^{116}Sn$ to the metastable state, $^{117m}Sn$, did not present a problem as adequate time (2 days) was allowed for decay to the ground state. Using the cadmium difference method permitted isolation of both a resonance integral and an average thermal neutron cross section. The CLICIT is cadmium lined and is assumed to reduce the thermal neutron flux component to an insignificant value due to cadmium's large thermal cross section of 2520 ± 50 b (Mughabghab, 1981).

Neglecting the thermal component allows direct calculation of the resonance integral to a very close approximation using a slightly varied form of Equation 3.2 presented here as Equation 3.3.

$$RI \approx A_o/[N\,(1-\exp(-\lambda\, t_{irr}))\,\varphi_{epi}] \qquad (3.3)$$

$RI \equiv$ resonance integral (b)
$\varphi_{epi} \equiv$ epithermal neutron flux ($cm^{-2}s^{-1}$)

It is important to note that this value is dependent on the RI of the selected flux monitor, $^{58}Fe$ in this case. All RI values used in calculations were measured over the epithermal energy range using the standard 0.5 eV to 100 keV integration limits. Once the RI is known, it can be used in Equation 3.4 to calculate the average thermal cross section.

$$\sigma_{th} \approx A_o/[N\,(1\text{-}\exp(-\lambda\, t_{irr}))\,\varphi_{th}\,] - [\varphi_{epi}\,(RI\,/\sigma_{th})] \qquad (3.4)$$

$\sigma_{th} \equiv$ average thermal neutron cross section (b)
$\varphi_{th} \equiv$ thermal neutron flux ($cm^{-2}s^{-1}$)

### 3.5.2 NEUTRON-PROTON REACTONS

Equation 3.2 was used to calculate the average cross section for the three (n,p) reactions studied. "There are two aspects involved in the analysis of neutron cross sections: (a) the kinematics of two particle collisions and (b) the dynamics of nuclear reactions" (Duderstadt, 1976). Principally, these two components, also called *kinematic* and *quantum* mechanics, determine whether or not a particle will be emitted following neutron absorption into the target nucleus, or if the process will end in neutron capture, (n, $\gamma$).

As previously alluded to in Chapter 2, kinematic and quantum mechanics determine the reaction threshold energy. While the following sections may be appropriately included in Chapter 4 as part of the Results and Discussion, they are presented here to aid in understanding the methods employed in establishing the correct limits of summation for the flux unfolding procedure to be discussed later in this chapter.

### 3.5.2.1 KINEMATIC MECHANICS

Kinematic mechanics involve the energy difference between the sum total of the masses of the reactants and the masses of the products. The energy equivalent of this mass difference is called a Q-value and is given by Equation 3.5 for the reaction A (a, b) B. Q-values were calculated for each reaction and reported in Chapter 2.

$$Q = (M_A + M_a - M_b - M_B)\ 931.48\ \text{MeV/amu} \qquad (3.5)$$

$M_A \equiv$ mass of target atom
$M_a \equiv$ mass of incident particle (neutron)
$M_b \equiv$ mass of resultant atom
$M_B \equiv$ mass of the emitted particle (hydrogen atom)

Two of the three (n,p) reactions have positive Q-values. If the Q-value is zero or positive, then the reaction is said to be exothermic and classical physics can be applied to show the reaction can occur with an incident neutron of zero kinetic energy. Conversely, reactions with negative Q-values are endothermic and the kinetic energy of the incident neutron must be sufficiently high to supply the excess energy required to satisfy the mass-energy imbalance, as is the case for the $^{91}$Zr (n,p) $^{91}$Y reaction. A negative Q-value, corrected for conservation of momentum using Equation 3.6, yields the kinematic threshold energy ($E_{th}$). This is the energy required to satisfy collision mechanics such that the proton can be emitted.

$$E_{th} = -Q\ (M_b + M_B)/(M_b + M_B - M_a) \qquad (3.6)$$

As can be seen by Equation 3.6, $E_{th}$ will always be slightly greater than the absolute value of the Q-value. For example, the Q-value for the $^{91}Zr$ (n,p) $^{91}Y$ reaction is -0.76165 MeV and the $E_{th}$ is 0.77070 MeV. While kinematics must be satisfied, (n,p) reaction thresholds are generally determined by quantum mechanics.

### 3.5.2.2 QUANTUM MECHANICS

From a kinematic standpoint, a positive Q-value means that no threshold exists. However, while possible to have a thermal neutron drive the (n,p) reaction, quantum mechanics tells us that the probability of the reaction occurring is practically zero. Quantum mechanics must also be satisfied. When one of the reactants is a charged particle and is near the nucleus – a mass of positively charged particles – a Coulomb barrier exists and must be penetrated or passed over. This barrier is depicted in Figure 3.2.

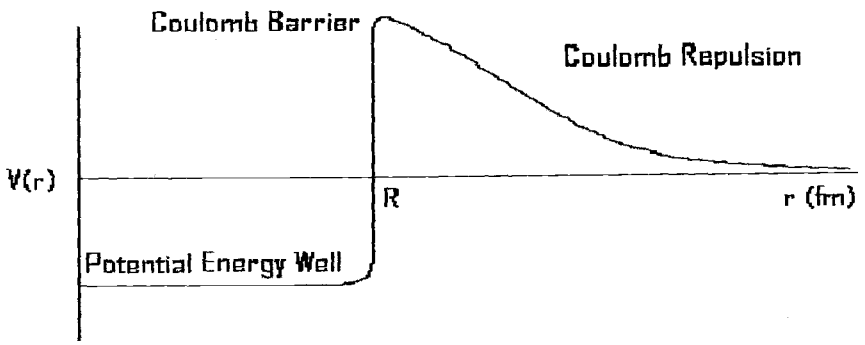


Figure 3.2. Graph of a typical Coulomb repulsive potential, V(r), versus radius, r, and the Coulomb barrier presented to a charged particle emitted from the nucleus.

The magnitude, or height, of this barrier can be calculated by Equation 3.7. Quantum mechanics allow for particles that lack sufficient energy to make it over the top of the barrier to penetrate through the barrier. The barrier transmission probability (TP) can be calculated using Equation 3.8.

$$V_{out} = \frac{z_b Z_b e^2 c}{4\pi\varepsilon_o c\ R} \tag{3.7}$$

$$TP = e^{-\left(\sqrt{\frac{8mz_b^2 Z_b^2 e^4 c^2}{(4\pi\varepsilon_o)^2 \hbar^2 c^2 E}}\right)\left[\left(\cos^{-1}\sqrt{\frac{R}{r'}}-\sqrt{\frac{R}{r'}-\frac{R^2}{r'^2}}\right)\right]} \tag{3.8}$$

$z_b \equiv$ charge of emitted particle
$Z_b \equiv$ charge of compound nucleus
$c \equiv$ speed of light
$\frac{e^2}{4\pi\varepsilon_o \hbar c} \equiv$ fine structure constant
$R \equiv$ radius of compound nucleus
$\hbar \equiv$ Planck's constant
$m \equiv$ mass of emitted particle
$E \equiv$ energy of incident emitted particle
$r' \equiv$ radius for which V(r')=E (see Figure 3.2)

Effectively this barrier presents the third, and usually largest, component when calculating an overall threshold energy required by incident particles to drive the reaction. The Coulomb barrier alone does not determine the overall threshold. Additionally, the availability of neutrons as predicted by the WFS and the material's cross section will "weigh in" to the overall threshold, as can be seen in Figure 3.3.

Figure 3.3. Plotted along with a normalized WFS are the actual and effective cross sections (effective is normalized), as well as and the product of the effective cross section (also normalized) versus Incident Neutron Energy for the $^{47}Ti(n,p)^{47}Sc$ reaction. The various thresholds associated with cross section measurements are shown for each cross section curve.

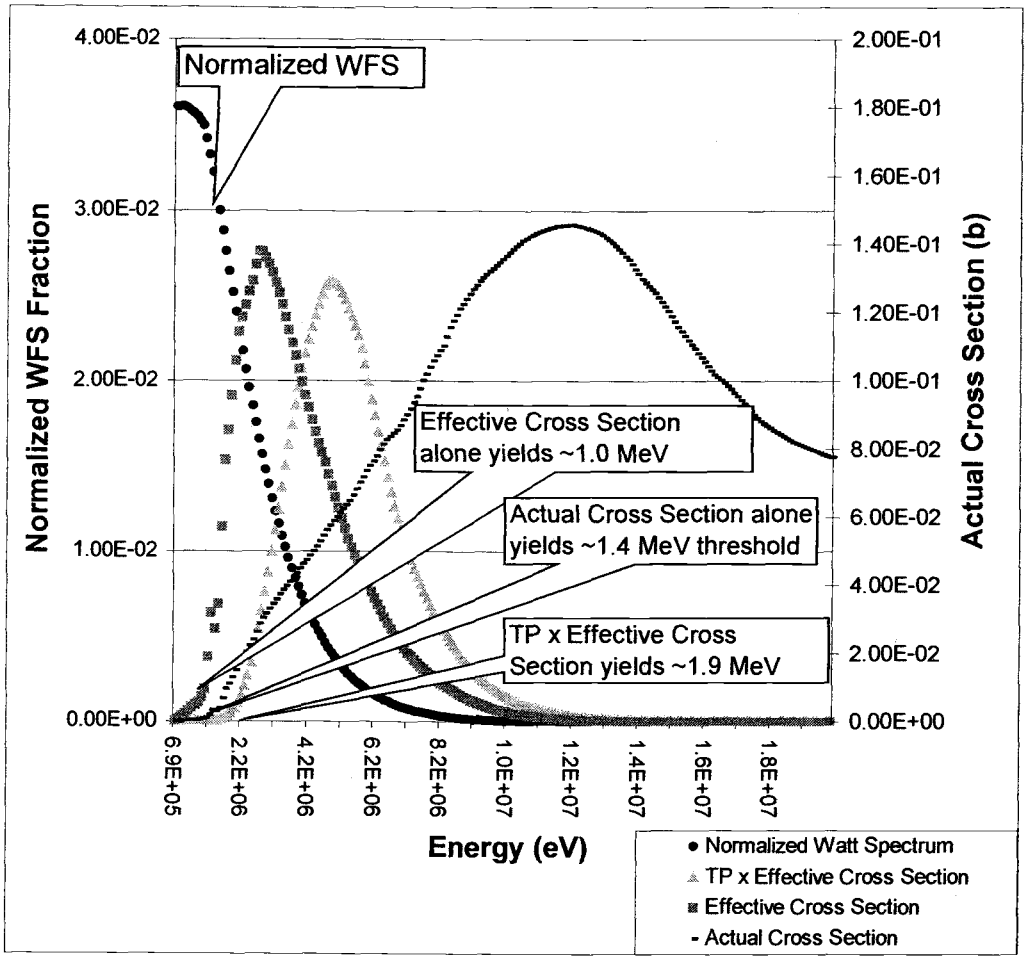


By multiplying the actual cross section at a given energy by the transmission probability for that energy and finally by the fraction of neutrons available at that energy as predicted by the WFS, an *effective* cross section emerges. The effective cross section is a contrived value with little physical meaning other than when plotted versus energy, it gives the overall threshold. Obviously, the cross section, which is the

probability of a reaction occurring, need not be weighted with another probability. In fact, the cross section is an empirically measured quantity that has the transmission probability imbedded in the measured value.

O'Brien (1969) reported an "effective threshold energy" of 4.7 MeV for the $^{67}Zn(n,p)^{67}Cu$ reaction even though he noted in his report that Van Loef (1961) had earlier reported a cross section of less than 5 mb at 3.3 MeV. Essentially the *effective threshold* is the energy at which the cross section has risen to a substantial value and efficient isotope production begins. Visually, this is just beyond the initial steep increase in the cross section as the curve "flattens out" and approaches its peak value. For national labs where accelerator time is at a premium, time on the accelerator will not be wasted. Only neutron energies above the effective threshold will be used in isotope production.

The concept of "efficient isotope production" makes little sense in terms of a thermal reactor where a continuum of neutron energies always exists and certain energies cannot easily be selectively discriminated. In most cases, it is appropriate to integrate over the entire fission spectrum, or at least above the kinematic threshold. Still, quantum threshold energies do become important when trying to unfold the fission spectrum and more precise limits of integration are required to pin down the energy at which the reaction becomes probable.

Much time was spent choosing the most correct threshold energy as proper unfolding of the flux is contingent upon knowing where the threshold reaction is exactly. Further evidence that this new method to determine an overall threshold has

merit is the comparison of effective threshold values from Baard et al. (1998) to energies calculated for 3% TP (Table 3.1).

Table 3.1. Comparison of various threshold values (*Baard, 1989).

| Reaction | Kinematic Threshold (MeV) | Coulomb Barrier (MeV) | Baard* Threshold (MeV) | TP = 3% (MeV) | TP = 1% (MeV) |
|---|---|---|---|---|---|
| $^{47}Ti(n,p)^{47}Sc$ | 0.00 | 5.58 | *2.30* | *2.25* | 1.87 |
| $^{54}Fe(n,p)^{54}Mn$ | 0.00 | 6.34 | *2.80* | *2.83* | 2.40 |
| $^{58}Ni(n,p)^{58}Co$ | 0.00 | 6.69 | *2.70* | *2.72* | 2.27 |
| $^{67}Zn(n,p)^{67}Cu$ | 0.00 | 6.84 | - | 3.07 | 2.62 |
| $^{91}Zr(n,p)^{91}Y$ | 0.77 | 8.31 | - | 5.09 | 4.56 |

Table 3.2. Ratio of cross sections evaluated at 1% Coulomb barrier transmission probability to the average fission cross section. (a) Values were "back calculated" to give approximately the same ratio as the top three reactions since they could not be accurately discerned from the cross section plot. These values are very close to the expected values based on visual extrapolation of the plots. Average fission cross section from (b) Mirzadeh (1986) and (c) ENDF/B-VI (Nuclear, 1994).

| Reaction | TP = 1% (MeV) | Cross Section at TP = 1% (mb) | Average Fission Cross Section (mb) | Ratio of Cross Sections (TP1% / AvgFis) |
|---|---|---|---|---|
| $^{47}Ti(n,p)^{47}Sc$ | 1.87 | 15 | 22.4 [c] | 0.670 |
| $^{54}Fe(n,p)^{54}Mn$ | 2.40 | 55 | 81.1 [c] | 0.678 |
| $^{58}Ni(n,p)^{58}Co$ | 2.27 | 70 | 106.5 [c] | 0.657 |
| $^{67}Zn(n,p)^{67}Cu$ | 2.62 | *0.71* [a] | 1.07 [b] | *0.664* |
| $^{91}Zr(n,p)^{91}Y$ | 4.56 | *0.16* [a] | 0.239 [c] | *0.669* |

Table 3.2 provides even more evidence to support the use of the 1% TP. When the cross section corresponding to the 1% TP threshold energy is divided by the average fission spectrum cross section, a nearly constant ratio results. The full meaning of why this ratio is nearly constant is not well understood, but it can be said that 1% TP threshold seems to be hinged in some way to the average value of the cross section. This provides another indication that the 1% TP is representative of the cross sections behavior with energy. For the purposes of this research, it was decided that demonstrated consistency in setting the limits of integration was paramount to maintaining the integrity of the experimental method. For this reason, the one-percent Coulomb barrier transmission probability was chosen as the overall threshold, or the energy at which the reaction becomes not only possible, but – more importantly – probable.

## 3.6 FLUX MONITORS

Two types of flux monitors were required. $^{58}Fe(n, ,\gamma)^{59}Fe$ was used to unfold the thermal and epithermal flux using the cadmium difference method. $^{54}Fe(n,p)^{54}Mn$, $^{58}Ni(n,p)^{58}Co$, and $^{60}Ni(n,p)^{60}Co$ reactions were used to unfold the fission spectrum. The use of each flux monitor to unfold the thermal, epithermal, and fast neutron energy spectrums will be described here, with more detail to follow in Chapter 5.

### 3.6.1 THERMAL AND EPITHERMAL FLUX MONITOR

Equations 3.3 and 3.4 can easily be solved for the epithermal and thermal flux components. Then, using a known resonance integral and thermal cross section, the epithermal and thermal flux can be directly calculated from a measured activity, in this case activity from the $^{58}Fe(n,\gamma)^{59}Fe$ reaction. Well-known cross sections for similar reactions occurring within the same elemental sample, such as $^{112}Sn(n, \gamma)^{113}Sn$, were also measured; this provided a self-regulating check of the experimental procedure. It was thought that if these measurements showed good agreement with their published cross sections, then greater confidence in the measured flux and resultant $^{116}Sn(n,\gamma)^{117m}$ cross sections is demonstrated.

### 3.6.2 FISSION SPECTRUM FLUX MONITOR UNFOLDING PROCEDURE

To measure the fission neutron spectrum several integral measurements, such as foil activities, were used to calculate the neutron spectrum. This procedure for obtaining the neutron spectrum is called unfolding. It is impossible to determine the neutron spectrum from a finite number of measured values, so a reasonably accurate assumed spectral shape must be employed (Sekimoto, 1978). At the International Specialists Symposium on Neutron Standard and Applications it was stated that the Watt distribution spectrum should be the recommended parametrization" (Stewart,

1977). Bresesti (1970) also "concluded that the Watt spectrum is the most appropriate representation of the $^{235}U$ fission spectrum."

Since the exact OSTR flux profile is not known, a methodology to "pin" a measured flux to a WFS generated profile was used. The methodology is as follows:

1. Using a spreadsheet, an energy band of 0.5 eV to 14.918 MeV with bin widths ($\Delta E$) of 1 keV was developed.
2. The Watt equation was evaluated at each energy to calculate the fraction of neutrons populating each energy. These fractions were normalized.
3. Using an iterative method a "pin" factor was calculated that produced the same flux over the same energy band as that measured for the threshold reaction flux monitors ($^{54}Fe(n,p)^{54}Mn$, $^{58}Ni(n,p)^{58}Co$, and $^{60}Ni(n,p)^{60}Co$).

## 3.7 DATA COMPARISON AND EVALUATION

All of the calculated cross sections were then compared to published values to determine if there is sufficient agreement or cause for further study. Cross sections were measured and reported with their associated error. When properly weighted using known threshold reactions to unfold the fluence distribution for the OSTR, these values will be accurate to the degree the WFS accurately approximates the actual OSTR flux. The assumption that the WFS exactly profiles the OSTR flux distribution will introduce a small measure of systemic error; however, this error is small

compared to that of the random errors associated with counting statistics and will be ignored. Relevant activation and dosimetric files used in quantitative analyses are available via the Internet. The most recent cross section data found for comparison was retrieved from the Internet based nuclear data libraries (ENDF/B, JEFF, JENDL, BROND, CENDL). More detail on the data libraries used in this research is provided in the Appendix.

# RESULTS

## 4.1 GENERAL OVERVIEW

The experimental results are listed in Tables 4.1 through 4.9. All data used in this research are presented with the associated error unless the error was not listed in the source information. The source information for all data that is not the result of a calculation or measurement is the National Nuclear Data Center's website (http://www.nndc.bnl.gov/), unless specifically noted otherwise.

The tabulations of the results are presented in a particular order. The top table on each page gives the target and parent isotopic data used in calculations. The bottom of each page gives the actual findings with some comparison values to aid in interpretation of the results. The first two tables list the data for the flux monitor used in the epithermal/thermal flux measurements ($^{58}$Fe). The first table lists the CLICIT results followed with the ICIT results. Two more tables for the $^{117m}$Sn, the reaction that used those flux measurements, follow these two tables.

The neutron-proton reaction results are presented next, starting off with two tables for the CLICIT, then ICIT flux monitor measurements. Following these tables, the three reactions are presented in order of atomic mass ($^{47}$Ti, $^{67}$Zn, and $^{91}$Zr). Since the neutron-proton reactions had fewer decay gammas to tabulate, both the CLICIT and ICIT data are presented together on the same page in the same table.

Each section of results will be fully discussed in Chapter 5. Only the data are presented here.

## 4.2 COMPARISON TERMS DESCRIBED

Specific Activity (SA) is the activity produced per unit mass of the sample. Ratio of SA is useful in noting the trend of flux depression between the ICIT and CLICIT, as well as a large discrepancy in the SA produced in one facility when compared to the other. The expectation is that these values are slightly greater than unity for the neutron-proton reactions, but can be more or less for the neutron-gamma reactions depending on how the reaction rates compare.

Specific Saturation Activity (SSA) is the SA achieved if the sample were to be irradiated for an infinite period of time, or the maximum possible value of activity per unit mass that could be produced under a given flux. SSA was used to depict the viability of low flux thermal reactor (e.g. OSTR) production of the isotope. Realize that in a larger flux the SSA will be larger as well. Also, the SSA is a theoretical value that is approached as the irradiation time goes to infinity. In other words, some percentage of SSA will be achieved in some finite time period, and this value can be calculated directly from SSA to determine the feasibility of production in a facility similar to the OSTR.

The comparators described up to this point are designed to help the reader get a "feel" for the degree of agreement between the data. They also helped the researcher

troubleshoot abnormalities to establish greater consistency in the data. Next, the key results, flux or cross section measurements, are presented in a more straightforward ratio. This comparison is a simply a ratio of the measured value to a "known" value.

## 4.3 RESULT TABULATIONS

Table 4.1. $^{58}Fe(n,\gamma)^{59}Fe$ CLICIT: (Top)Reaction data and counting information used in activity calculations. (Bottom) Comparisons of measured activity and measured flux values.

| Reaction (CLICIT) | Sample Weight (mg) | Sample AW (g) | Isotopic Abund. (%) | Half-life (d) | Gamma Energy (keV) | Branch Ratio | Net Counts | Detector Efficiency | Irrad. Time (s) | Decay Time (s) | Count Time (s) |
|---|---|---|---|---|---|---|---|---|---|---|---|
| $^{58}Fe(n,\gamma)^{59}Fe$ (1099 keV) | 52.3 | 55.845 | 0.28 ± 0.01 | 44.503 ± 0.006 | 1099.251 ± 0.004 | 0.565 ± 0.015 | 35,775 ± 203 | 0.00202 ± 0.000236 | 10,860 | 253,020 | 7,200 |
| $^{58}Fe(n,\gamma)^{59}Fe$ (1292 keV) | 52.3 | 55.845 | 0.28 ± 0.01 | 44.503 ± 0.006 | 1291.596 ± 0.007 | 0.432 ± 0.011 | 24,147 ± 161 | 0.00179 ± 0.000213 | 10,860 | 253,020 | 7,200 |

| Reaction (CLICIT) | Measured Activity (Bq) | TRIGA Specific Saturation Activity (MBq/mg) | Ratio of Specific Activity ($SA_{ICIT}$:$SA_{CLICIT}$) | Measured $\varphi_{epi}$ ($n/cm^2s$) | OSTR Historical $\varphi_{epi}$ ($n/cm^2s$) | Ratio of $\varphi_{epi}$ ($\varphi_{epi\ Meas}$: $\varphi_{epi\ Hist}$) |
|---|---|---|---|---|---|---|
| $^{58}Fe(n,\gamma)^{59}Fe$ (1099 keV) | $4.57x10^3$ | 0.0447 | 7.33 | $9.97x10^{11}$ ± $1.33x10^{11}$ | $1.0x10^{12}$ | 0.997 |
| $^{58}Fe(n,\gamma)^{59}Fe$ (1292 keV) | $4.55x10^3$ | 0.0445 | 7.26 | $9.93x10^{11}$ ± $1.34x10^{11}$ | $1.0x10^{12}$ | 0.993 |
| $^{58}Fe(n,\gamma)^{59}Fe$ (Weighted Average) | $4.56x10^3$ | 0.0446 | 7.30 | $9.95x10^{11}$ ± $1.34x10^{11}$ | $1.0x10^{12}$ | 0.995 |

Table 4.2. $^{58}Fe(n,\gamma)^{59}Fe$ ICIT: (Top)Reaction data and counting information used in activity calculations. (Bottom) Comparisons of measured activity and measured flux values.

| Reaction (ICIT) | Sample Weight (mg) | Sample AW (g) | Isotopic Abund. (%) | Half-life (d) | Gamma Energy (keV) | Branch. Ratio | Net Counts | Detector Efficiency | Irrad. Time (s) | Decay Time (s) | Count Time (s) |
|---|---|---|---|---|---|---|---|---|---|---|---|
| $^{58}Fe(n,\gamma)^{59}Fe$ (1099 keV) | 52.3 | 55.845 | 0.28 ± 0.01 | 44.503 ± 0.006 | 1099.251 ± 0.004 | 0.565 ± 0.015 | 86,715 ± 305 | 0.00197 ± 0.000234 | 10,800 | 267,900 | 7,200 |
| $^{58}Fe(n,\gamma)^{59}Fe$ (1292 keV) | 52.3 | 55.845 | 0.28 ± 0.01 | 44.503 ± 0.006 | 1291.596 ± 0.007 | 0.432 ± 0.011 | 57,819 ± 242 | 0.002 ± 0.0002 | 10,800 | 267,900 | 7,200 |

| Reaction (ICIT) | Measured Activity (Bq) | TRIGA Specific Saturation Activity (MBq/mg) | Ratio of Specific Activity ($SA_{ICIT}$:$SA_{CLICIT}$) | Measured $\varphi_{th}$ ($n/cm^2s$) | OSTR Historical $\varphi_{th}$ ($n/cm^2s$) | Ratio of $\varphi_{th}$ ($\varphi_{th\ Meas}$: $\varphi_{th\ Hist}$) |
|---|---|---|---|---|---|---|
| $^{58}Fe(n,\gamma)^{59}Fe$ (1099 keV) | $1.13x10^4$ | 0.330 | 7.33 | $9.19x10^{12}$ ± $1.37x10^{12}$ | $1.0x10^{13}$ | 0.919 |
| $^{58}Fe(n,\gamma)^{59}Fe$ (1292 keV) | $1.12x10^4$ | 0.325 | 7.26 | $9.04x10^{12}$ ± $1.37x10^{12}$ | $1.0x10^{13}$ | 0.904 |
| $^{58}Fe(n,\gamma)^{59}Fe$ (Weighted Average) | $1.13x10^4$ | 0.327 | 7.30 | $9.11x10^{12}$ ± $1.37x10^{12}$ | $1.0x10^{13}$ | 0.911 |

Table 4.3. $^{116}Sn(n,\gamma)^{117m}Sn$ CLICIT: (Top) Reaction data and counting information used in activity calculations. (Bottom) Comparison of measured activities and measured RI to the evaluated ENDF/B-VI RI (NEA, 1994). (a) Resonance integral for radiative capture to the metastable state could not be found for ENDF/B-VI, so the value listed in the book of Neutron Cross Sections was used instead (Mughabghab et al., 1981).

| Reaction (CLICIT) | Samp Wght (mg) | Sample AW (g) | Isotope Abund. (%) | Half-life (d) | Gamma Energy (keV) | Branch. Ratio | Net Counts | Detector Efficiency | Irrad. Time (s) | Decay Time (s) | Cnt Time (s) |
|---|---|---|---|---|---|---|---|---|---|---|---|
| $^{116}Sn(n,\gamma)^{117m}Sn$ | 14.1 | 118.71 | 14.53 ± 0.01 | 13.6 ± 0.04 | 158.562 ± 0.012 | 0.86 | 5,489,760 ± 2524 | 0.0105 ± 0.00101 | 10,860 | 164,640 | 7,200 |
| $^{112}Sn(n,\gamma)^{113}Sn$ (255 keV) | 14.1 | 118.71 | 0.97 ± 0.01 | 115.09 ± 0.04 | 255.05 ± 0.03 | 0.0182 ± 0.0006 | 15,756 ± 195 | 0.00732 ± 0.000752 | 10,860 | 164,640 | 7,200 |
| $^{112}Sn(n,\gamma)^{113}Sn$ (391 keV) | 14.1 | 118.71 | 0.97 ± 0.01 | 115.09 ± 0.04 | 391.68 ± 0.015 | 0.64 | 411,689 ± 672 | 0.00528 ± 0.000575 | 10,860 | 164,640 | 7,200 |

| Reaction (CLICIT) | Measured Activity (Bq) | TRIGA Specific Saturation Activity (MBq/mg) | Ratio of Specific Activity ($SA_{ICIT}$:$SA_{CLICIT}$) | Measured RI (b) | ENDF/B-VI RI (b) | Ratio of Cross Sections ($RI_{meas}$:$RI_{tab}$) |
|---|---|---|---|---|---|---|
| $^{116}Sn(n,\gamma)^{117m}Sn$ | $9.32 \times 10^4$ | 1.03 | 1.18 | 1.41 ± 0.23 | 0.49[a] ± 0.16 | 2.88 |
| $^{112}Sn(n,\gamma)^{113}Sn$ (255 keV) | $1.66 \times 10^4$ | 1.56 | 1.29 | 31.8 ± 5.5 | 29.72 | 1.07 |
| $^{112}Sn(n,\gamma)^{113}Sn$ (391 keV) | $1.71 \times 10^4$ | 1.60 | 1.16 | 32.8 ± 5.7 | 29.72 | 1.10 |

Table 4.4. $^{116}Sn(n,\gamma)^{117m}Sn$ ICIT: (Top) Reaction data and counting information used in activity calculations. (Bottom) Comparison of measured activities and the measured $\sigma_{th}$ to the evaluated ENDF/B-VI $\sigma_{th}$ (NEA, 1994). (a) Thermal capture cross section for radiative capture to the metastable state could not be found for ENDF/B-VI, so the value listed in the book of Neutron Cross Sections was used instead (Mughabghab et al., 1981).

| Reaction (ICIT) | Samp Wght (mg) | Sample AW (g) | Isotope Abund. (%) | Half-life (d) | Gamma Energy (keV) | Branch. Ratio | Net Counts | Detector Efficiency | Irrad. Time (s) | Decay Time (s) | Cnt Time (s) |
|---|---|---|---|---|---|---|---|---|---|---|---|
| $^{116}Sn(n,\gamma)^{117m}Sn$ | 14.8 | 118.71 | 14.53 ± 0.01 | 13.6 ± 0.04 | 158.562 ± 0.012 | 0.86 | 5,710,318 ± 2442 | 0.00891 ± 0.00107 | 10,800 | 180,780 | 7,200 |
| $^{112}Sn(n,\gamma)^{113}Sn$ (255 keV) | 14.8 | 118.71 | 0.97 ± 0.01 | 115.09 ± 0.04 | 255.05 ± 0.03 | 0.0182 ± 0.0006 | 17,567 ± 213 | 0.00604 ± 0.000777 | 10,800 | 180,780 | 7,200 |
| $^{112}Sn(n,\gamma)^{113}Sn$ (391 keV) | 14.8 | 118.71 | 0.97 ± 0.01 | 115.09 ± 0.04 | 391.68 ± 0.015 | 0.64 | 404,385 ± 680 | 0.00425 ± 0.000580 | 10,800 | 180,780 | 7,200 |

| Reaction (ICIT) | Measured Activity (Bq) | TRIGA Specific Saturation Activity (MBq/mg) | Ratio of Specific Activity ($SA_{ICIT}$:$SA_{CLICIT}$) | Measured $\sigma_{th}$ (b) | ENDF/B-VI $\sigma_{th}$ (b) | Ratio of Cross Sections ($\sigma_{th\ meas}$: $\sigma_{th\ tab}$) |
|---|---|---|---|---|---|---|
| $^{116}Sn(n,\gamma)^{117m}Sn$ | $1.15 \times 10^5$ | 1.23 | 1.18 | 0.0287 ± 0.0224 | 0.006[(a)] ± 0.002 | 4.78 |
| $^{112}Sn(n,\gamma)^{113}Sn$ (255 keV) | $2.22 \times 10^4$ | 1.99 | 1.27 | 0.977 ± 0.618 | 1.018 | 0.898 |
| $^{112}Sn(n,\gamma)^{113}Sn$ (391 keV) | $2.09 \times 10^4$ | 1.88 | 1.16 | 0.661 ± 0.579 | 1.018 | 0.650 |

Table 4.5. CLICIT (n,p): (Top) Data used in activity calculations. (Bottom) Comparisons of measured activity and flux.

| Reaction (CLICIT) | Samp Wght (mg) | Samp AW (g) | Isotope Abund. (%) | Half-life (d) | Gamma Energy (keV) | Branch. Ratio | Net Counts | Detector Efficiency | Irrad. Time (s) | Decay Time (s) | Cnt Time (s) |
|---|---|---|---|---|---|---|---|---|---|---|---|
| $^{54}Fe(n,p)^{54}Mn$ | 52.3 | 55.84 | 5.8 ± 0.1 | 312.3 ± 0.4 | 834.848 ± 0.004 | 0.99976 ± 0.00001 | 127,002 ± 381 | 0.00248 ± 0.000280 | 10,860 | 253,020 | 7,200 |
| $^{58}Ni(n,p)^{58}Co$ (811 keV) | 21.1 | 58.69 | 68.077 ± 0.009 | 70.86 ± 0.07 | 810.775 ± 0.009 | 0.99 | 4,486,126 ± 2155 | 0.00304 ± 0.000363 | 10,860 | 234,600 | 7,200 |
| $^{58}Ni(n,p)^{58}Co$ (864 keV) | 21.1 | 58.69 | 68.077 ± 0.009 | 70.86 ± 0.07 | 863.959 ± 0.009 | 0.00683 ± 0.00011 | 28,851 ± 199 | 0.00289 ± 0.000348 | 10,860 | 234,600 | 7,200 |
| $^{58}Ni(n,p)^{58}Co$ (1675 keV) | 21.1 | 58.69 | 68.077 ± 0.009 | 70.86 ± 0.07 | 1674.73 ± 0.01 | 0.00518 ± 0.00008 | 12,394 ± 116 | 0.00175 ± 0.000228 | 10,860 | 234,600 | 7,200 |

| Reaction (CLICIT) | Measured Activity (Bq) | TRIGA Specific Saturation Activity (MBq/mg) | Ratio of Specific Activity ($SA_{ICIT}$:$SA_{CLICIT}$) | Measured $\varphi_{rxn}$ ($n/cm^2s$) | Threshold Energy $E_{th}$ (MeV) | Percent of Fission Neutrons $E_n > E_{th}$ |
|---|---|---|---|---|---|---|
| $^{54}Fe(n,p)^{54}Mn$ | $7.17x10^3$ | 0.543 | 1.10 | $9.69x10^{12}$ ± $1.20x10^{12}$ | 2.40 | 30.8% |
| $^{58}Ni(n,p)^{58}Co$ (811 keV) | $2.13x10^5$ | 8.21 | 1.09 | $1.10x10^{13}$ ± $1.43x10^{12}$ | 2.27 | 33.4% |
| $^{58}Ni(n,p)^{58}Co$ (864 keV) | $2.08x10^5$ | 8.03 | 1.12 | $1.08x10^{13}$ ± $1.42x10^{12}$ | 2.27 | 33.4% |
| $^{58}Ni(n,p)^{58}Co$ (1675 keV) | $1.95x10^5$ | 7.53 | 1.16 | $1.01x10^{13}$ ± $1.42x10^{12}$ | 2.27 | 33.4% |
| $^{58}Ni(n,p)^{58}Co$ (Wgtd Avg) | $2.05x10^5$ | 7.92 | 1.12 | $1.07x10^{13}$ ± $1.42x10^{12}$ | 2.27 | 33.4% |

Table 4.6. ICIT Flux Monitors: (Top) Data used in activity calculations. (Bottom) Comparisons of measured activity and flux.

| Reaction (ICIT) | Samp Wght (mg) | Samp AW (g) | Isotope Abund. (%) | Half-life (d) | Gamma Energy (keV) | Branch. Ratio | Net Counts | Detector Efficiency | Irrad. Time (s) | Decay Time (s) | Cnt Time (s) |
|---|---|---|---|---|---|---|---|---|---|---|---|
| $^{54}Fe(n,p)^{54}Mn$ | 17.7 | 55.84 | 5.8 ± 0.1 | 312.3 ± 0.4 | 834.848 ± 0.004 | 0.99976 ± 0.00001 | 46,429 ± 327 | 0.00243 ± 0.000279 | 10,800 | 267,900 | 7,200 |
| $^{58}Ni(n,p)^{58}Co$ (811 keV) | 6.5 | 58.69 | 68.077 ± 0.009 | 70.86 ± 0.07 | 810.775 ± 0.009 | 0.99 | 1,166,431 ± 1105 | 0.00234 ± 0.000351 | 10,800 | 249,480 | 7,200 |
| $^{58}Ni(n,p)^{58}Co$ (864 keV) | 6.5 | 58.69 | 68.077 ± 0.009 | 70.86 ± 0.07 | 863.959 ± 0.009 | 0.00683 ± 0.00011 | 7,614 ± 133 | 0.00223 ± 0.000273 | 10,800 | 249,480 | 7,200 |
| $^{58}Ni(n,p)^{58}Co$ (1675 keV) | 6.5 | 58.69 | 68.077 ± 0.009 | 70.86 ± 0.07 | 1674.73 ± 0.01 | 0.00518 ± 0.00008 | 3,262 ± 59 | 0.00130 ± 0.000178 | 10,800 | 249,480 | 7,200 |

| Reaction (ICIT) | Measured Activity (Bq) | TRIGA Specific Saturation Activity (MBq/mg) | Ratio of Specific Activity ($SA_{ICIT}$:$SA_{CLICIT}$) | Measured $\varphi_{rxn}$ ($n/cm^2s$) | Threshold Energy $E_{th}$ (MeV) | Percent of Fission Neutrons $E_n > E_{th}$ |
|---|---|---|---|---|---|---|
| $^{54}Fe(n,p)^{54}Mn$ | $2.67x10^3$ | 0.543 | 1.10 | $1.07x10^{13} \pm 1.34x10^{12}$ | 2.40 | 30.8% |
| $^{58}Ni(n,p)^{58}Co$ (811 keV) | $7.18x10^4$ | 9.04 | 1.09 | $1.22x10^{13} \pm 1.92x10^{12}$ | 2.27 | 33.4% |
| $^{58}Ni(n,p)^{58}Co$ (864 keV) | $7.16x10^4$ | 9.01 | 1.12 | $1.21x10^{13} \pm 1.63x10^{12}$ | 2.27 | 33.4% |
| $^{58}Ni(n,p)^{58}Co$ (1675 keV) | $6.95x10^4$ | 8.75 | 1.16 | $1.18x10^{13} \pm 1.75x10^{12}$ | 2.27 | 33.4% |
| $^{58}Ni(n,p)^{58}Co$ (Wgtd Avg) | $7.09x10^4$ | 8.93 | 1.12 | $1.20x10^{13} \pm 1.75x10^{12}$ | 2.27 | 33.4% |

Table 4.7. $^{47}Ti(n,p)^{47}Sc$: (Top) Comparison of measured activities and the measured $\sigma_{rxn}$ to the evaluated ENDF/B-VI $\sigma_{rxn}$ (NEA, 1994). (Bottom) Reaction data and counting information used in activity calculations.

| Reaction | Samp Wght (mg) | Samp AW (g) | Isotope Abund. (%) | Half-life (d) | Gamma Energy (keV) | Branch Ratio | Net Counts | Detector Efficiency | Irrad. Time (s) | Decay Time (s) | Count Time (s) |
|---|---|---|---|---|---|---|---|---|---|---|---|
| $^{47}Ti(n,p)^{47}Sc$ (CLICIT) | 9.0 | 91.22 | 7.30 ± 0.1 | 3.3492 ± 0.0006 | 159.377 ± 0.012 | 0.683 ± 0.004 | 8,985,274 ± 3106 | 0.00856 ± 0.000777 | 10,860 | 175,500 | 60,000 |
| $^{47}Ti(n,p)^{47}Sc$ (ICIT) | 8.5 | 91.22 | 7.30 ± 0.1 | 3.3492 ± 0.0006 | 159.377 ± 0.012 | 0.683 ± 0.004 | 10,435,767 ± 3283 | 0.00860 ± 0.000791 | 10,800 | 190,320 | 60,000 |

| Reaction | Measured Activity (Bq) | TRIGA Specific Saturation Activity (MBq/mg) | Ratio of Specific Activity ($SA_{ICIT}$:$SA_{CLICIT}$) | Measured $\sigma_{rxn}$ (mb) | ENDF/B-VI $\sigma_{rxn}$ (mb) | Ratio of Cross Sections ($\sigma_{rxn\ meas}$: $\sigma_{rxn\ tab}$) |
|---|---|---|---|---|---|---|
| $^{47}Ti(n,p)^{47}Sc$ (CLICIT) | $4.18 \times 10^4$ | 0.192 | 1.13 | 15.5 ± 1.6 | 22.36 | 0.69 |
| $^{47}Ti(n,p)^{47}Sc$ (ICIT) | $5.01 \times 10^4$ | 0.218 | 1.13 | 15.7 ± 8.0 | 22.36 | 0.70 |

Table 4.8. $^{67}Zn(n,p)^{67}Cu$: (Top) Comparison of measured activities and the measured $\sigma_{rxn}$ to the value Mirzadeh reported as the widely adopted value (1986). (Bottom) Reaction data and counting information used in activity calculations.

| Reaction | Samp Wght (mg) | Samp AW (g) | Isotope Abund. (%) | Half-life (h) | Gamma Energy (keV) | Branch Ratio | Net Counts | Detector Efficiency | Irrad. Time (s) | Decay Time (s) | Count Time (s) |
|---|---|---|---|---|---|---|---|---|---|---|---|
| $^{67}Zn(n,p)^{67}$ Cu (CLICIT) | 66.2 | 65.39 | 4.10 ± 0.01 | 61.83 ± 0.12 | 184.577 ± 0.01 | 0.487 ± 0.003 | 130,681 ± 1569 | 0.00767 ± 0.000710 | 10,860 | 179,340 | 7,200 |
| $^{67}Zn(n,p)^{67}$ Cu (ICIT) | 24.7 | 65.39 | 4.10 ± 0.01 | 61.83 ± 0.12 | 184.577 ± 0.01 | 0.487 ± 0.003 | 43,176 ± 785 | 0.00769 ± 0.000723 | 10,800 | 179,340 | 7,200 |

| Reaction | Measured Activity (Bq) | TRIGA Specific Saturation Activity (MBq/mg) | Ratio of Specific Activity ($SA_{ICIT}$:$SA_{CLICIT}$) | Measured $\sigma_{rxn}$ (mb) | Widely Accepted $\sigma_{rxn}$ (mb) | Ratio of Cross Sections ($\sigma_{rxn\ meas}$: $\sigma_{rxn\ tab}$) |
|---|---|---|---|---|---|---|
| $^{67}Zn(n,p)^{67}$ Cu (CLICIT) | $6.44x10^3$ | 0.00293 | 1.18 | 1.07 ± 0.113 | 1.07 | 1.00 |
| $^{67}Zn(n,p)^{67}$ Cu (ICIT) | $2.83x10^3$ | 0.00346 | 1.18 | 1.06 ± 0.115 | 1.07 | 0.99 |

Table 4.9. $^{91}Zr(n,p)^{91}Y$: (Top) Comparison of measured activities and the measured $\sigma_{rxn}$ to the evaluated ENDF/B-VI $\sigma_{rxn}$ (NEA, 1994). (Bottom) Reaction data and counting information used in activity calculations. (a) Sample counts were below background levels; a MDA calculation was used to determine the largest possible peak, and, therefore, the largest possible cross section.

| Reaction [a] | Samp Wght (mg) | Samp AW (g) | Isotope Abund. (%) | Half-life (d) | Gamma Energy (keV) | Branch Ratio | Net Counts [a] | Detector Efficiency | Irrad. Time (s) | Decay Time (s) | Count Time (s) |
|---|---|---|---|---|---|---|---|---|---|---|---|
| $^{91}Zr(n,p)^{91}Y$ (CLICIT) | 23.7 | 91.224 | 11.22 ± 0.04 | 58.51 ± 0.06 | 1204.77 ± 0.06 | 0.003 | N/A | 0.00188 ± 0.000222 | 10,800 | 153,120 | 7,200 |
| $^{91}Zr(n,p)^{91}Y$ (ICIT) | 22.7 | 91.224 | 11.22 ± 0.04 | 58.51 ± 0.06 | 1204.77 ± 0.06 | 0.003 | N/A | 0.00184 ± 0.000221 | 10,800 | 168,000 | 7,200 |

| Reaction [a] | Measured Activity [a] (Bq) | TRIGA Specific Saturation Activity [a] (MBq/mg) | Ratio of Specific Activity [a] ($SA_{ICIT}$:$SA_{CLICIT}$) | Measured $\sigma_{rxn}$ [a] (mb) | ENDF/B-VI $\sigma_{rxn}$ (mb) | Ratio of Cross Sections [a] ($\sigma_{rxn\ meas}$: $\sigma_{rxn\ tab}$) |
|---|---|---|---|---|---|---|
| $^{91}Zr(n,p)^{91}Y$ (CLICIT) | Assumed MDA ($8.17x10^3$) | < 0.232 | 0.846 | < 140 ± 26 | 0.2389 | < 587 |
| $^{91}Zr(n,p)^{91}Y$ (ICIT) | Assumed MDA ($6.63x10^3$) | < 0.197 | 0.846 | < 106 ± 22 | 0.2389 | 4< 45 |

# DISCUSSION

## 5.1 $^{58}Fe(n,\gamma)^{59}Fe$ EPITHERMAL AND THERMAL FLUX MEASUREMENTS

As can be seen from Table 4.1, there exists strong agreement between the flux calculated from each of the $^{59}Fe$ decay gammas. The 1099 keV (56.5%) and 1292 keV (43.2%) gamma peaks yield resultant flux values that agree within 0.5%. Also, considering that the error-weighted average of both values is within 5% of the historically accepted value for the OSTR ICIT indicates that the measured epithermal flux of $9.95 \times 10^{11}$ $cm^{-2}s^{-1}$ may be more accurate than the associated error of $\pm$ $1.34 \times 10^{11}$ (one sigma) would suggest.

The "error-weighted average" is a normalized weighting coefficient that weights each measured value inversely by the square of its own error (Knoll, 1989). The weighting factor (w) can be calculated using Equation 5.1, where $\sigma_x$ represents the individual errors.

$$w_j = \frac{1}{\sigma_{x_j}^2}\left(\sum_{i=1}^{N}\frac{1}{\sigma_{x_i}^2}\right)^{-1} \tag{5.1}$$

Table 4.2 gives the thermal flux, or ICIT, data and results. Again, excellent agreement between the flux derived from each gamma (within 5%), and the error-weighted average is within 10% of the historically accepted value. It is believed that

this value is more accurate than the historical value as it represents the actual flux for this experiment. A value of $9.11 \times 10^{12} \pm 1.34 \times 10^{12}$ $cm^{-2} s^{-1}$ (one sigma) is a reasonable value for the thermal flux.

## 5.2 $^{116}Sn(n,\gamma)^{117m}Sn$ CROSS SECTION MEASUREMENTS

The epithermal resonance integral measurement results (listed in Table 4.3) are reasonably good considering the relative size of the gamma peaks observed. The 159 keV peak was adjacent to the other $^{59}Fe$ decay peak (156 keV) that made resolution somewhat difficult. It was decided that both could not be resolved so the more prevalent of the two was analyzed. The resultant cross section of $1.41 \pm 0.49$ b (one sigma) is reasonable. While this is 2.9 times larger than the value listed in Mughabghab et al. (1981), there exists very little literature to support that value of $0.49 \pm 0.16$ b. This is partly because RI measurements for production of metastable isotopes are less common. It may also be due to the inability to completely resolve the adjacent gamma peaks.

As can be seen by the inclusion of the two $^{113}Sn$ gammas on Table 4.3, the counting statistics agree very well. There is also good agreement between the ratios of specific activities (SA), which lends more credibility to the $^{117m}Sn$ results. The fact that the $^{113}Sn$ gammas show good agreement with tabulated cross section values (within 10%), and that the $^{117m}Sn$ has about the same SA ratio extends greater

confidence to the $^{59}$Fe counting statistics even though only one $^{117m}$Sn gamma was analyzed for the RI measurement.

The average thermal cross section measurement is similarly high and is almost five times larger than that listed in Mughabghab et al. (1981). The delicate balance between the coupled measured epithermal RI and the measure thermal average cross section leads to low confidence in this result. The resultant thermal average cross section of 28.7 ± 2.2 mb (one sigma) is precariously perched on the verge of becoming a negative result if the RI gamma peak is integrated over a slightly larger area. Careful selection of the proper bounds for peak count summation was required to achieve a positive answer. This measurement would best be done in the OSTR Thermal Column irradiation facility.

## 5.3 $^{54}$Fe(n,p)$^{54}$Mn AND $^{58}$Ni(n,p)$^{58}$Co

### 5.3.1 FLUX UNFOLDING

As described in Chapter 3, the $^{54}$Fe(n,p)$^{54}$Mn and $^{58}$Ni(n,p)$^{58}$Co threshold reactions were used to unfold the flux. The quality of the counting statistics for those reactions will be discussed in the next section. This section will discuss the accuracy and results of unfolding the fast neutron, or fission spectrum. Remember that "the true fission spectrum is considerably depleted below 1 MeV" and not well represented by the WFS in that region (Grundl, 1968). Accordingly, the WFS is purported to be most

accurate above 1 MeV even though it has a most probable energy of ~0.72 MeV. Since an energy profile characterized by the WFS is an undisturbed fission spectrum, any perturbations in the flux reduce its accuracy. The "piling up" of moderated neutrons below 1 MeV leads to a reduction in accuracy in that region as well. Real life constraints dictate that most irradiation facilities are not located within the fuel region but are, however, as close to the fuel as practically possible.

The fact that a WFS characterized neutron profile does not take into account that the irradiation facility is not located exactly where the neutrons are produced introduces a systemic error. This error will bias the results to some degree. It is common practice to ignore this error as it cannot be avoided and is usually small compared to random errors associated with the activation technique. Also, using a normalized WFS tends to overcome this bias since a magnitude is not introduced by the characterization, only a flux shape. Perturbations in the flux shape can only be more closely approximated through transport calculations as previously discussed.

The ICIT and CLICIT facilities are located within the core and are separated from the fuel by approximately one inch of water. This leads to softening of the fission spectrum in the moderator and, when coupled with the previously discussed problem of reduced accuracy of the WFS at energies below 1 MeV, it could result in an overstated fast flux profile if the $^{58}Fe$ flux monitor were used instead of a threshold reaction flux monitor. In other words, due to moderation of the neutron spectrum there will be more epithermal neutrons than those directly produced from fission. This

is why it is imperative that the flux be unfolded to accurately depict the neutron population at energies above the threshold.

Threshold limits of summation were determined for each reaction as described earlier, and were based on a 1% Coulomb barrier transmission probability. The normalized WFS calculated over fast neutron energy range (0.5 eV to ~ 15 MeV) was multiplied by a scalar pin factor. The name "pin factor" stems from the fact that this scalar is used to "pin" the flux at two points. The WFS was pinned at 2.40 MeV for $^{54}$Fe(n,p) and 2.27 MeV for $^{58}$Ni(n,p). The scalar was chosen to return flux values equal to the measured flux values when multiplied times the normalized WFS and summed from the respective threshold values to 15 MeV. The agreement in the pinned flux and the measured flux for both the $^{54}$Fe(n,p) and $^{58}$Ni(n,p) reactions was less than 2% in the ICIT and less than 1% in the CLICIT.

While this is excellent agreement the fact that the two threshold energies are only 0.13 MeV apart deflates any overconfidence that may result. However, if the WFS accurately depicts the fission spectrum, and most experts agree it does, then any one quality flux measurement should be able to fix the entire spectrum. The fact that the present research presents two independent values with excellent agreement only improves the confidence in these results. With that said, future studies should choose flux monitors with a better spread of threshold energies.

### 5.3.2 $^{54}Fe(n,p)^{54}Mn$ AND $^{58}Ni(n,p)^{58}Co$ FLUX MEASUREMENTS

Iron is an excellent choice as a flux monitor, aiding in the resolution of the thermal, epithermal, and fission spectra. As can be seen from Tables 4.5and 4.6, the $^{54}Mn$ and $^{58}Co$ decay gammas produce excellent counting peaks. Also, the agreement between the $^{58}Co$ gammas was remarkable considering the huge difference in branching ratios: 99% (811 keV) and less than 1% (864 and 1675 keV). Ratio of specific activities showed excellent agreement, as do the measured flux values relative to the percentage of the fission spectrum they each represent. The $^{58}Ni$ represents approximately 2.6% more neutrons and should be slightly higher. The measured flux values meet this expectation.

The ICIT flux was also slightly greater than the CLICIT flux as would be expected due to a slight flux depression caused by the cadmium. The ICIT and CLICIT values agreed within 10% lending a good degree of confidence to the accuracy and precision of the measurement. All reported flux measurement errors are one sigma errors and are the result of rigorous tracking of each contribution to the overall error.

## 5.4 $^{47}Ti(n,p)^{47}Sc$ CROSS SECTION MEASUREMENTS

The ICIT and CLICIT titanium samples showed excellent agreement both returning a measured average fission cross section of approximately 15.6 mb.

Accordingly, all ratios show excellent agreement. Also, the sample was counted again after approximately nine days of decay time and again returned nearly the same value (1.3 % difference) for the resultant cross section. The only concern with this value is that there exists much literature that suggests the 22.4 mb value is correct. There are two plausible explanations: (1) the data, which would be an indication of a systemic error that would result in the lowering of all the data, or (2) previous studies have not adequately studied the lower energy portion of the fission spectrum. The latter is the more likely of the two considering the excellent agreement other results have show with the adopted values. It may be that the 22.4 mb cross section is inflated by the preponderance of experimental evidence at higher energies that would suggest a larger cross section since the cross section increases with energy. This warrants further investigation.

## 5.5 $^{67}Zn(n,p)^{67}Cu$ CROSS SECTION MEASUREMENTS

A consistent ratio of SA ranging from 1.10 to 1.18 between the ICIT and CLIC suggests good counting statistics. The originally measured values were slightly less than the "widely adopted value of 1.07 mb" reported by Mirzadeh (1986), but greater than any other reported value that was found in literature. Interestingly enough, after a long decay time (~ 9 days) both the resultant ICIT and CLICIT fission average cross sections were 1.06 ± 0.115 mb (one sigma) and 1.07 ± 0.113 mb (one sigma),

respectively. It is believed that these are the more correct of the two measurements and were reported as the fission average cross section in Table 4.8.

## 5.6 $^{91}Zr(n,p)^{91}Y$ CROSS SECTION MEASUREMENTS

The expected single gamma peak for Zr at 1205 keV (0.3%) was not observed. Instead, the background counts were measured across the energy region where the peak would have been. The width of a nearby peak (1202.7 keV) was used to approximate a peak width for determining background counts. The background counts were then used to calculate a Minimum Detectable Activity (MDA). The MDA was used in turn to determine the largest possible peak that could go undetected. The calculated MDA was then used to calculate the largest possible cross section.

As can be seen from Table 4.9, the results are poor. The "largest possible" cross section was ~ 500 times larger than the expected value of 0.2389 mb. It is not certain why the peak was not observed or why the background was so high in that region, but it was surmised that it had something to do with the higher energy. Cross sections of the expected magnitude were measured by this research; however, they were all low energy peaks that would more readily interact with the germanium detector. Measurement of this cross section might give better results if the detector was calibrated for the higher energy.

# CONCLUSION

With little knowledge of the actual OSTR flux profile, a methodology was proven to "pin" the profile and accurately measure cross sections. It was also shown that appreciable amounts of medical isotopes could be produced in low flux thermal reactors. The fission average cross section for the $^{67}Zn(n,p)$ reaction of $1.07 \pm 0.113$ mb (one sigma) was found to be larger than the value found in much of the literature. $^{47}Ti(n,p)$ yielded a $15.5 \pm 1.6$ mb (one sigma) fission average cross section, which is slightly less than the widely adopted value of 22.4 mb.

Concerning nuclear data, there is a continuous need for improvements, according to the new trends in nuclear medicine and materials research. Neutron Activation Analysis (NAA) relevant data regarding thermal neutron capture cross sections and resonance integrals are in constant need of being updated.

Future work should include more cross section measurements, but first a code should be purchased and used to conduct a more precise unfolding of the neutron spectrum. This would benefit much of the research performed with the OSTR. Also, there is a lack of information concerning threshold reactions and how "effective thresholds" are determined. This would make an excellent thesis in and of itself.

# REFERENCES

ASTM; Standard Practice for Determining Fluence, Fluence Rate, and Spectra by Radioactivation Techniques. Designation E 261-98. West Conshohocken, PA; 1997.

ASTM; Standard Test Method for Determining Thermal Neutron Reaction and Fluence Rates by Radioactivation Techniques. Designation E 262-97; West Conshohocken, PA; 1998.

Baard, J. H., Zijp, W. L., Nolthenius, H. J.; Nuclear Data Guide for Reactor Neutron Metrology; Netherlands Energy Research Foundation ECN; Petten, Netherlands; 1989.

Binney, S.E. Nuclear and Radiation Physics: An Overview to Nuclear Engineering. Lecture Notes. Department of Nuclear Engineering Oregon State University; 1987.

Binney, S.E. Principles of Nuclear Medicine. Lecture Notes. Department of Nuclear Engineering Oregon State University; 2002.

Bresesti, A.M.; Bresesti, M.; Rota, A.; Rydin, R.A. Threshold Reaction Excitation Functions Intercalibrated in a Pure Fission Spectrum. Nuclear Chemistry Laboratory, C.C.R EURATOM; Ispra, Italy; 1970.

CSEWG: Cross Section Evaluation Working Group. ENDF-102 Data Formats and Procedures for The Evaluated Nuclear Data File ENDF-6. National Nuclear Data Center Brookhaven National Laboratory; Upton, New York; 2001.

Duderstadt, J.J.; Hamilton, L.J. Nuclear Reactor Analysis. Department of Nuclear Engineering: The University of Michigan; Ann Arbor, Michigan; 1976.

Fast Flux Test Facility Desperately Needed For Medical Isotopes. August 2001. http://www.medicalisotopes.org/docs/desperate.html

General Electric and Lockheed Martin; Nuclides and Isotopes, Fifteenth Edition, Chart of the Nuclides; 1996.

Grundl, J.A. "Brief Review of Integral Measurements with Fission Spectrum Neutrons," *Proc. Consultants Mtg. Prompt Fission Neutron Spectra*, Vienna, Austria, August 25-27, 1972, STI/ PUB/ 329, p. 29, International Atomic Energy Agency (1972).

Knoll, G. F. Radiation Detection and Measurement: Second Edition. Professor of Nuclear Engineering: The University of Michigan; Ann Arbor, Michigan; 1979, 1989.

Kocher, D. C. Radioactive Decay Data Tables, A Handbook of Decay for Application to Radiation Dosimetry and Radiological Assessment; DOE/TIC-11026; 1981.

Lederer, C. M.; Shirley, V.S. Table of Isotopes: Seventh Edition. Lawrence Berkeley Laboratory University of California, Berkeley; 1978.

Mannhart, W. Neutron Activation Cross Sections for Fission and Fusion Energy Applications. Argonne National Laboratory, Argonne, Illinois; September 13-15, 1989.

Mausner, L. F.; Mirzadeh, S.; Srivastava, S.C. Improved Specific Activity of Reactor Produced $^{117m}$Sn with Szilard-Chalmers Process. Medical Department, Brookhaven National Laboratory; Upton, New York; October 1991.

McLane, V., Dunford, C. L., Rose, P. F.; Neutron Cross Sections: Volume 2. Neutron Cross Section Curves. National Nuclear Data Center Brookhaven National Laboratory; Upton, New York; 1988.

Mellish, C.E., Payne, and Otlet. Flux and Cross Section Measurements with Fast Fission Neutrons in BEPO and DIDO, Report AERE I/R 2630, Atomic Energy Research Establishment, Harwell (1958).

Mirzadeh, S., Mausner, L. F., Srivastava, S. C.; Production of No-Carrier Added $^{67}Cu$; Medical Department, Brookhaven National Laboratory; Upton, New York; June 1986.

Mughabghab, S. F.; Divadeenam, M.; Holden, N.E. Neutron Cross Sections: Volume 1. Neutron Resonance Parameters and Thermal Cross Sections; Part A: Z=1-60. National Nuclear Data Center Brookhaven National Laboratory; Upton, New York; 1981.

Nesaraja, C.; Linse, K.H.; Spellerberg, S.; Sudar, S.; Suhaimi, A.; Qaim, S.M. Excitation Functions of Neutron Induced Reactions on some Isotopes of Zinc, Gallium and Germanium in the Energy Range of 6.2 to 12.4 MeV. Institute for Nuclear Chemistry; Julich, Germany; 1999.

Nuclear Energy Agency Organization for Economic Co-Operation and Development. Table of Simple Integral Neutron Cross Section Data from JEF-2.2, ENDF/B-VI, JENDL-3.2, BROND-2 and CENDL-2. Head of Publications Service, OECD; 1994.

O'Brien, H.A. The Preparation of $^{67}Cu$ from $^{67}Zn$ in a Nuclear Reactor. Isotopes Development Center, Oak Ridge National Laboratory; Oak Ridge, Tennessee; August 1968.

Philis, C.; Bersillon, O.; Smith, D.; Smith, A. Nuclear Data and Measurements Series. Evaluated (n,p) Cross Sections of $^{46}Ti$, $^{47}Ti$, and $^{48}Ti$. Argonne National Laboratory; Argonne, Illinois; January 1977.

Qaim, S.M. Neutron Activation Cross-Section Measurements on Zirconium, Niobium and Molybdenum in the Energy Range of 4 to 10 MeV Using Radiochemical Techniques. Institute for Nuclear Chemistry; Julich, Germany; 1990.

Raloff, J. Wanted: Medical Isotopes. Overcoming a Critical Scarcity of Radioactive Materials for Research. October 1999. http://www.sciencenews.org/sn_arc99/10_23_99/bob1.htm

Sekimoto, H. A Direct Technique for Unfolding Neutron Spectra from Activation Data. Research Laboratory for nuclear Reactors, Tokyo Institute of Technology; O-okayama, Meguro-ku, Tokyo, Japan; 1978

Smith, D.L.; Meadows, J.W. Nuclear Data and Measurements Series: Cross Sections for (n,p) Reactions on $^{27}Al$, $^{46,47,48}Ti$, $^{54,56}Fe$, $^{58}Ni$, $^{59}Co$, and $^{64}Zn$ from Near Threshold to 10 MeV. Argonne National Laboratory; Argonne, Illinois; January 1975.

Stewart, L., and Eisenhauer, C.M.: "Prompt Fission Neutron Spectra", Neutron Standards and Applications, Proc. Symp. Gaithersburg, MD (1977), NBS Special Publ. 493, 198 (NBS, Gaithersburg, MD, 1977).

Wagner, M.; Vonach, H. Neutron Activation Cross Sections for Fission and Fusion Energy Applications. Argonne National Laboratory, Argonne, Illinois; September 13-15, 1989.

# APPENDIX

# LIST OF COMMON CROSS SECTION LIBRARIES

**ADL-3**

Russian activations data library released in 1993. The library contains 20,049 excitation functions of reactions on stable and unstable targets for neutron energies up to 20 MeV. The library is in a pseudo ENDF-6 format, i.e., it generally follows ENDF formatting rules, but with some modifications to allow description of reactions leading to metastable states.

**BROND-2.2**

Russian evaluated neutron data library, issued in 1992 and updated in 1993. Library is in ENDF-6 format and contains data for 121 materials from 1-H-1 to 96-Cm-244.

**CENDL-2.1**

Chinese evaluated neutron data library issued in 1991, updated and supplemented in 1993 and 1995. The library is in ENDF-6 format and contains data for 67 materials from 1-H-1 to 98-Cf-249.

**ENDF/B-VI (release 8)**

US evaluated nuclear data library released in 1990, with revisions in 1991, 1993, 1995, 1996, 1998, 1999, 2000 and 2002. The library is divided into the following sublibraries: incident neutron data (general purpose library), radioactive decay data, fission yield data, thermal scattering law data, photo-atomic interaction data, incident charged-particle data, activation data, and dosimetry data. Two high-energy data libraries also exist, containing neutron and proton reaction data up to 1 GeV incident energy. The general purpose library is in ENDF-6 format and contains data for 440 materials from 1-H-1 to 99-Es-253, with approximately 30 materials having evaluations up to 150 MeV. The proton sublibrary has been significantly increased and now contains 34 evaluations.

**JEFF-3.0**

The joint evaluated Fission and Fusion File (JEFF-3.0) is an evaluated library produced via an international collaboration of data bank member countries co-ordinated under the auspices of the NEA Data Bank. The JEFF-3.0 library comprises at present only a general purpose library including thermal scattering law data for 5 materials. This general purpose library was released in April 2002. It is in ENDF-6 format and contains data for 340 materials from 1-H-1 to 99-Es-255.

**JENDL-3.3**

Japanese Evaluated Neutron Data Library, released in 2002. The library is ENDF-6 format and contains data for 337 materials from 1-H-1 to 100-Fm-255.